

AD A113740

12 07

EXPERIMENTAL INVESTIGATION OF THE FREE ELECTRON LASER

F.A. Dolezal, R.J. Harvey, A.J. Palmer

C.G. Parazzoli

Hughes Research Laboratories
3011 Malibu Canyon Road
Malibu, CA 90265

Hughes Electro-Optical and
Data Systems Division

February 1982

N00014-79-C-0957

Final Report

For Period 21 September 1979 through 31 December 1981

Approved for public release; distribution unlimited.

Sponsored by
OFFICE OF NAVAL RESEARCH
Arlington, VA 22217

DTIC
APR 23 1982
H

82 04 23 004

UNCLASSIFIED

SECURITY CLASSIFICATION OF THIS PAGE (When Data Entered)

REPORT DOCUMENTATION PAGE		READ INSTRUCTIONS BEFORE COMPLETING FORM
1. REPORT NUMBER	2. GOVT ACCESSION NO.	3. RECIPIENT'S CATALOG NUMBER
	AD-A113 740	
4. TITLE (and Subtitle) Experimental Investigation of the Free Electron Laser		5. TYPE OF REPORT & PERIOD COVERED Final Report 9/21/79 - 12/31/81
		6. PERFORMING ORG. REPORT NUMBER
7. AUTHOR(s) F.A. Dolezal, R.J. Harvey, A.J. Palmer, and C.G. Parazzoli		8. CONTRACT OR GRANT NUMBER(s) N00014-79-C-0957
9. PERFORMING ORGANIZATION NAME AND ADDRESS Hughes Research Laboratories 3011 Malibu Canyon Road Malibu, CA 90265		10. PROGRAM ELEMENT, PROJECT, TASK AREA & WORK UNIT NUMBERS
11. CONTROLLING OFFICE NAME AND ADDRESS U.S. Navy Office of Naval Research Arlington, VA 22217		12. REPORT DATE February 1982
		13. NUMBER OF PAGES
14. MONITORING AGENCY NAME & ADDRESS (if different from Controlling Office)		15. SECURITY CLASS. (of this report) Unclassified
		15a. DECLASSIFICATION DOWNGRADING SCHEDULE
16. DISTRIBUTION STATEMENT (of this Report) Approved for public release; distribution unlimited.		
17. DISTRIBUTION STATEMENT (of the abstract entered in Block 20, if different from Report)		
18. SUPPLEMENTARY NOTES		
19. KEY WORDS (Continue on reverse side if necessary and identify by block number) Free Electron Laser Low Voltage Free Electron Laser Beam Electron Gun Depressed Collector Brillouin Flow Monochromaticity Thomson Scattering		
20. ABSTRACT (Continue on reverse side if necessary and identify by block number) An e-gun, depressed collector and guide-field solenoid has been designed for operation at a maximum of 400 kV and 38 A. The results of experiments with this brassboard system include demonstration of depressed collector recovery efficiencies of over 90% for e-beam voltages from 160 to 300 keV and currents up to 25 A. We have also confirmed Hughes computer-code predictions that a space-charge depression in the collector (which is essential to efficient collection) forms at a		

DTIC
EXTRACTED
APR 23 1982

UNCLASSIFIED

SECURITY CLASSIFICATION OF THIS PAGE(When Data Entered)

collector-voltage setting of 1% of the beam voltage. These results demonstrate the validity of substantially increasing the efficiency of FEL systems, by using depressed collectors to recover the bulk of the energy which is left in the e-beam after it leaves the laser resonator. Preliminary indications are that the recovery efficiency (recovered current/cathode-emission current) increases gradually with beam voltage (reaching 94% at 300 keV) as beam spreading due to thermal effects and sensitivity to the focusing-field strength are reduced. We expect to translate these results into FEL-system efficiencies of an order of magnitude higher per stage than would be possible without the use of depressed collection.

Techniques for measuring the monochromaticity of high quality ($\Delta E/E \sim 10^4$) e-beams were also examined. End-on Thomson scattering was identified as the most feasible technique for this measurement. A Thomson scattering experiment has been designed and hardware implemented into the brassboard system.

UNCLASSIFIED

SECURITY CLASSIFICATION OF THIS PAGE(When Data Entered)

FOREWORD

Scientific Officer for this program was Dr. Robert E. Behringer at ONR Pasadena. Contract Manager at Hughes was Mr. Frank A. Dolezal. The project was originally begun at the Electro-Optical and Data Systems Division, and was transferred to the Hughes Research Laboratories Division in September 1980.



Accession For	
NTIS GRA&I	<input checked="" type="checkbox"/>
DTIC TAB	<input type="checkbox"/>
Unannounced	<input type="checkbox"/>
Justification	
By _____	
Distribution/	
Availability Codes	
Dist	(Avail and/or Special)
A	

TABLE OF CONTENTS

SECTION		PAGE
1	INTRODUCTION AND SUMMARY.....	9
	A. Background.....	9
	B. Conceptual Approach.....	11
2	CRITICAL GAIN-RELATED ISSUES.....	15
3	ELECTRON GUN AND COLLECTOR DESIGN.....	21
	A. Electron Gun.....	21
	B. Brillouin Flow.....	23
	C. Segmented Cathode Approach.....	26
	D. Thermal Effects on Propagation.....	26
	E. Depressed Collector.....	28
4	ELECTRON BEAM MONOCHROMATICITY MEASUREMENT APPROACH.....	35
	A. Approaches.....	35
	B. Thomson Scattering From An Electron Beam.....	36
5	SYSTEM MECHANICAL AND ELECTRICAL DESIGN.....	47
	A. Overall System.....	47
	B. FEL Components.....	47
	C. Electronics.....	51
	D. Thomson Scattering.....	54
6	EXPERIMENTAL RESULTS.....	59
	A. Vacuum Chamber.....	59
	B. E-Gun.....	59
	C. Depressed Collector.....	63
	D. Thomson Scattering.....	78
7	SUMMARY.....	83
	REFERENCES.....	85

LIST OF ILLUSTRATIONS

FIGURE		PAGE
1	Conceptual design of a two-stage FEL.....	10
2	E-gun momentum spread reduction techniques.....	13
3	Oscillation conditions for a two-stage FEL.....	19
4	Electron beam monochromaticity requirement for Figure 3 oscillation condition.....	20
5	Typical computer plot of the equipotential lines and electron trajectories in the e-gun.....	22
6	Momentum spread as a function of radial position at the e-gun exit.....	25
7	Momentum spread as a function of radial position for segmented and unsegmented cathodes.....	27
8	Relevant electron trajectory plot for the baseline e-gun.....	29
9	Computer plot of the equipotential lines and electron trajectories in the depressed collector. Depressed collector voltage is 7 kV.....	30
10	Computer plot of the equipotential lines and electron trajectories in the depressed collector. Depressed collector voltage is 4 kV.....	31
11	Experimental layout of the Thomson scattering experiment.....	37
12	E-field and wave vectors for the Thomson scattering experiment.....	39
13	Thomson scattering intensity profile in the electron rest frame.....	41
14	Relativistic intensity enhancement as a function of scattering angle.....	44
15	Hughes FEL experimental set-up.....	48
16	System outline drawing.....	49
17	FEL components.....	50

PRECEDING PAGE BLANK-NOT FILMED

FIGURE		PAGE
18	Depressed collector cup.....	52
19	Electronic diagnostic circuit.....	52
20	Solenoid driver circuit.....	53
21	Pulse timing diagram.....	55
22	Timing and trigger generation circuits.....	56
23	Mass analyzer photos.....	60
24	Current voltage characteristic, $T_k = 1140^\circ\text{C}$	62
25	Typical e-gun current trace, $V_{\text{anode}} = 395 \text{ kV}$	64
26	Depressed collector response, $V_{\text{anode}} = 19 \text{ kV}$	66
27	Depressed collector current as a function of delay setting, $V_{\text{anode}} = 19 \text{ kV}$	67
28	Solenoid current as a function of mode number.....	68
29	Depressed collector voltage dependence, $V_{\text{anode}} = 19 \text{ kV}$	70
30	Depressed collector current versus guide field strength.....	71
31	Depressed collector current versus voltage.....	72
32	Depressed collector efficiency versus anode voltage.....	73
33	Collector efficiency versus magnetic field.....	74
34	Depressed collector efficiency versus collector voltage.....	76
35	Depressed collector efficiency (with axial hole) versus collector voltage.....	77
36	Thomson scattering concept.....	79
37	Detector response criteria.....	81
38	Laser temporal response.....	82

SECTION 1

INTRODUCTION

A. BACKGROUND AND SUMMARY

In principle, two-stage free electron lasers (FEL) require relatively low voltages (<10 MeV) to reach optical or near-infrared wavelengths.¹ One of the keys to the success of the development of low voltage FELs is the efficient generation, control and recovery of a highly monochromatic electron beam (e-beam). A conceptual design of a two-stage FEL is shown in Figure 1. Here a static-wiggler magnet is used to excite radiation from the first stage at the pump wavelength, λ_p . As the power density of the first stage field builds up to a high level ($\sim 10^8$ W/cm²), it begins to pump the second stage which radiates at the signal wavelength, λ_s . The gain and efficiency are important limiting factors to the operation of the second stage of FELs of this type. Variations in the longitudinal velocity of the e-beam determine the gain bandwidth. This variation must be kept small. The unused e-beam energy must be recovered in order to keep the overall FEL efficiency high. The objectives of the program were to characterize a high quality e-beam and to demonstrate an efficient depressed collector which is suitable to employ in two-stage FELs. The specific goals of this program were to demonstrate e-guns with velocity spreads less than one part in 10^{-4} and beam-energy-recovery systems with efficiencies of better than 95%.

In order to achieve these objectives and goals we first performed an extensive analysis of the design principles of e-guns and the propagation of e-beams. Design concepts were examined using computer code simulations. These were then translated into hardware designs for the electron gun and the depressed collector. Diagnostic techniques were also assessed; these influenced the test system designs as did the availability of power supplies and sensors. After several iterations we settled on end-on Thomson scattering as the most practical technique to measure the beam energy spread; although the beam voltage requirements of ≥ 400 keV are at the upper limit of the capability of the available apparatus. We assembled a test system having an operational 400-kV, 38-A e-gun, 1.3-m solenoidal-guide and focusing field, depressed

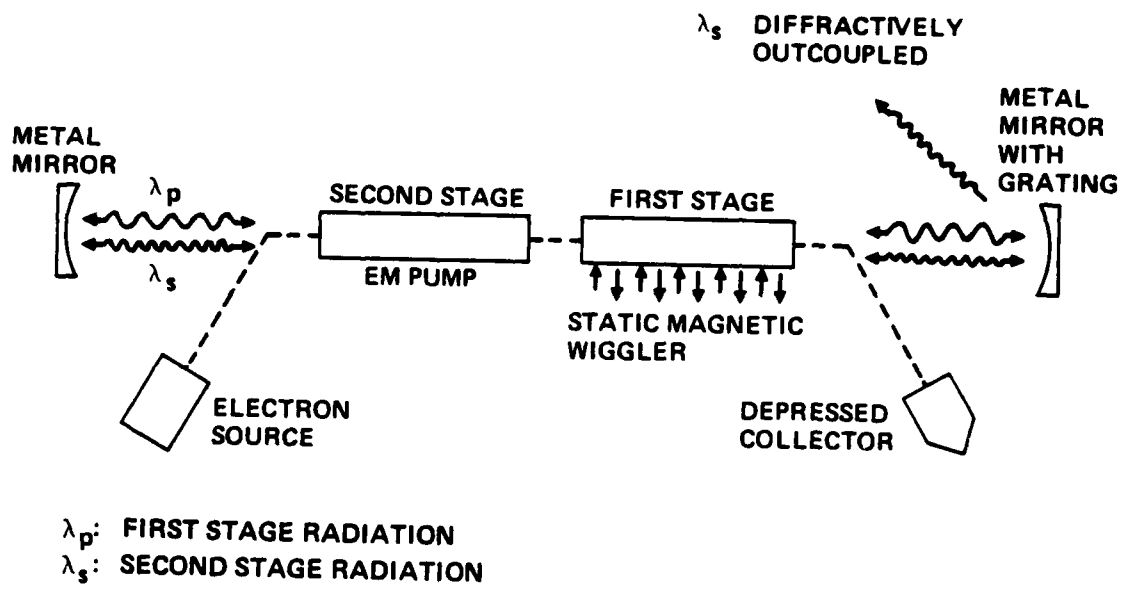


Figure 1. Conceptual design of two-stage FEL.

collector, 9.25- μ m CO₂ laser-probe beam and associated optical-diagnostic and system-control circuitry. We have been able to demonstrate depressed-collector-recovery efficiencies of over 90% for beam voltages from 160 to 300 keV and currents up to 25 A. We have also confirmed our computer-code predictions that a space-charge depression in the collector (which is essential to efficient collection) forms at a collector-voltage setting of 1% of the beam voltage. The beam-energy recovery efficiency (η = recovered current/cathode-emission current) increases gradually with beam voltage (reaching 94% at 300 keV) as beam spreading due to thermal effects and sensitivity to the focusing-field strength are reduced. These results imply that two-stage FELs can be designed with an overall FEL-system efficiency of more than two orders of magnitude higher than would be possible without the use of depressed collection.

Preliminary Thomson scattering experiments indicate that noise from background light and EMI are at sufficiently low levels to allow the experiment to proceed. Improvements in the reliability and repetition rate of the high voltage system are desirable in order to expedite the collection of data.

B. CONCEPTUAL APPROACH

The energy spread in the e-beam (or more precisely the longitudinal velocity distribution) may be due to several sources. For a beam generated by a conventional Pierce e-gun with a thermionic cathode, part of the energy spread originates in edge effects, cathode regions with low emission and in the finite envelope of emission angles near the cathode surface. These are amplified by aberrations in the gun and focusing optics. They may be reduced at the expense of the current by reducing the perveance ($\mathcal{P} \equiv I/V^{3/2}$) of the e-gun. The local value of the beam velocity is also related to the electric and magnetic fields produced by the beam itself. These self-field effects are related and are not reduced by the gun perveance. For a uniform cylindrical current distribution propagating in the drift region, the self-electrostatic potential, ϕ , varies quadratically with radius. The potential difference between the edge of the beam ($r = r_b$) and the center of the beam ($r = 0$) is proportional to the current. It is approximated by:

$$\Delta\phi = \frac{I}{4\pi\epsilon_0 c\beta} = \frac{30 I}{\beta} \text{ (mks units)} \quad (1)$$

This potential is the dominant contribution to the velocity spread at currents of more than a few amperes, when the cathode is operating fully space-charge limited. Since all of the electrons normally originate at the same potential, with near zero kinetic energy, their kinetic energies must differ by $\Delta E = e \Delta\phi$ across the beam, as shown in Figure 2(a). At the focal plane of the e-gun, the spread in the longitudinal momentum P_z is approximated by

$$\frac{\Delta P_z}{P_z} = \gamma^2 \frac{\Delta\beta_z}{\beta_z} = \frac{1}{\gamma \beta^2} \frac{\Delta E}{mc^2} = \frac{5.87 \times 10^{-5} I}{\gamma \beta^3} \quad (2)$$

This spread can be reduced in two ways:

- (1) **Segmented Cathode:** By changing the potential distribution across the cathode to cancel the effect of the self field. As illustrated in Figure 2(b), this approach may be approximated by segmenting the cathode in annular rings.
- (2) **Brillouin Flow:** By introducing an axial magnetic-focusing field which allows the axial velocities to be replaced by rotational velocity. As shown in Figure 2(c), it results in a solid-body rotation of the beam.

Neither approach can be implemented in its ideal form, and on a real FEL the effect of the wiggler field must be included. Nevertheless, we show below that significant improvements are predicted by analytical and computer simulations in each of these approaches. Combinations of these approaches may also be taken together to match to more arbitrary FEL system configurations.

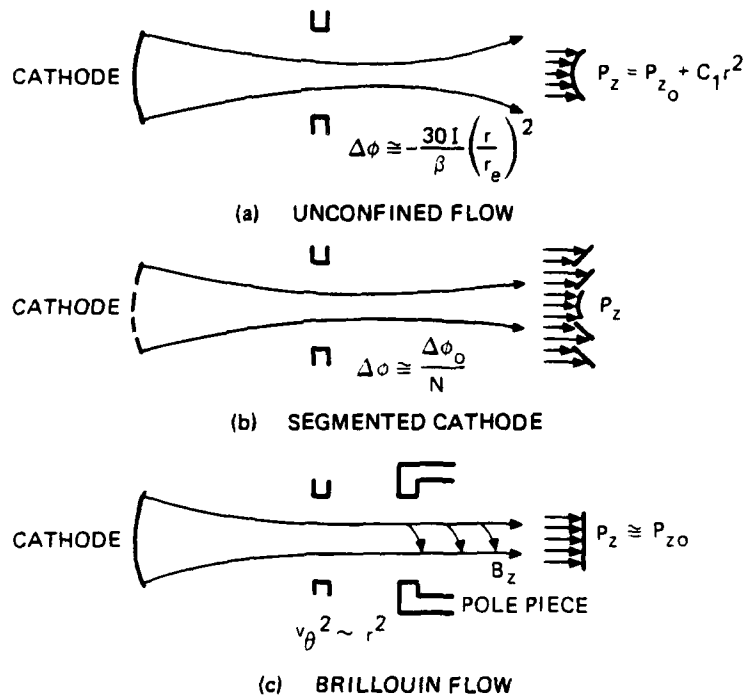


Figure 2. E-gun momentum-spread-reduction techniques.

SECTION 2

CRITICAL GAIN-RELATED ISSUES

The most important issue for the operation of a low voltage two-stage free electron laser is the small value of the gain coefficient. The second stage of a low voltage two-stage FEL will operate in the weak pump, single particle regime. The small-signal power-gain coefficient for an FEL operating in this regime is given approximately by:²

$$g(\text{m}^{-1}) = 4.2 \times 10^{-23} S F n_e \gamma^3 \lambda_s^3 \left(\frac{\Delta\omega}{\omega}\right)^{-2} \quad (3)$$

where:

S = pump power in W/m^2

F = area fill factor

n_e = electron beam density in $(\text{m})^{-3}$

γ = relativistic γ for the electron beam axial velocity

λ_s = signal wavelength (m)

$\frac{\Delta\omega}{\omega}$ = fractional gain linewidth

For the considered operating regime $\Delta\omega/\omega$ is the larger of either the homogeneous linewidth due to the finite length, ℓ , of the gain path,³

$$\Delta\omega/\omega_{\text{homogeneous}} = 2 \gamma^2 \lambda_s / \ell \quad (4)$$

or the inhomogeneous Doppler linewidth due to axial momentum spread, P_z , of the electrons^{2,4}

$$\Delta\omega/\omega_{\text{inhomogeneous}} = 2 \Delta P_z / P_z \quad (5)$$

Diffraction spreading of the wave vectors of both the pump and signal radiation will also contribute to the Doppler linewidth by an amount

$$\frac{\Delta\omega}{\omega}_{\text{diffraction}} \approx \left[\left(\frac{\beta}{1-\beta} \frac{\Theta_s^2}{2} \right)^2 + \left(\frac{\beta}{1+\beta} \frac{\Theta_p^2}{2} \right)^2 \right]^{1/2} \approx \frac{\Theta_p^2}{4} \quad (6)$$

where $\beta = v_z/c$, and the effective diffraction angles, Θ_i , are given approximately by

$$\Theta_i \approx \frac{2 \lambda_i}{W_i} F_i^{1/2} \quad (i = s, p) \quad (7)$$

where the subscripts on the wavelength, waist diameter (W_i) and fill factor (F_i) refer to the respective signal and pump radiation fields. This diffraction-induced linewidth is primarily due to pump-field diffraction and reduces to

$$\frac{\Delta\omega}{\omega}_{\text{diffraction}} \approx 16 \gamma^4 \lambda_s^2 / W^2 \text{ for } F_s = F_p = 1 \quad (8)$$

It must be kept smaller than the first two linewidths under the considered operating conditions.

Coherence limitations of the pump radiation can also contribute to the linewidth. These contributions remain smaller than the homogeneous linewidth given by Equation (4) provided the coherence length of the pump radiation is longer than the gain path. We assume this to be the case for this discussion.

It is also especially advantageous for the low-voltage two-stage FEL approach to keep ΔP_z small and operate in the homogeneously broadened regime.

We plot, in Figures 3 and 4, the conditions necessary to achieve a 1% per pass gain in the homogeneously broadened regime by using Equations (3-5). The values selected for the pump power were: $S = 10^{12} \text{ W/m}^2$, the electron density,

$n_e = 10^{16} \text{ m}^{-3}$, and the fill factor, $F = 1$. A gain of 1% per pass is assumed to be sufficient to achieve oscillation in an optical Fabre-Perot cavity in the wavelength range of interest.

In Figure 3 we plot the conditions for oscillation. We also show, with the dashed curve, the second-stage output wavelength versus e-beam energy of a two-stage free electron laser. Here the same e-beam energy is used throughout the laser and the second-stage pump radiation is the first-stage signal radiation derived from a static-magnetic-wiggler with a 2-cm period (as shown in Figure 3). Portions of the solid curve above the dashed curve require pump wavelengths longer than would be provided in this way while portions below the dashed curve require shorter wavelength pump radiation. Figure 4 plots the maximum momentum spread of the e-beam allowed in order for the oscillation curves of Figure 3 to be in the homogeneously broadened regime as assumed. Depending on whether the primary constraint is on e-beam energy or beam monochromaticity, Figure 3 or Figure 4 would be used to select the design point of the FEL. For example, if the beam monochromaticity is no better than 10^{-4} at 2 MeV, a 4- μm two-stage FEL could be built at the assumed pump power, fill factor, and beam density by using a gain path 70 cm or longer. From Figure 4 the second-stage beam voltage required would be 2 MeV.

For space-charge-dominated electron beams the current I is given in terms of beam diameter W by

$$I = n_e e c \beta \frac{\pi W^2}{4} \quad (9)$$

If no correction is made for the space-charge potential, it follows from Equation 2 that the space-charge potential contribution to the linewidth is

$$\frac{\Delta\omega}{\omega_{\text{inhomogeneous}}} = \frac{e^2 n_e W^2}{8\gamma\beta^2 \epsilon_0 m c^2} = \frac{\omega_p^2 W^2}{8\gamma\beta^2 c^2} \quad (\text{mks}) \quad (10)$$

where ω_p is the electron plasma frequency.

For a fixed-fill factor, the diffraction, and space-charge-inhomogeneous-broadening terms (Equation 8 and 10) are coupled by the beam diameter W . The minimum constraint occurs when they are both set equal to the homogeneous term, i.e.:

$$\frac{\Delta\omega}{\omega} \text{ homogeneous} = \frac{\Delta\omega}{\omega} \text{ inhomogeneous} = \frac{\Delta\omega}{\omega} \text{ diffraction} \quad (11)$$

This yields the conditions for matching the resonant cavity to the gain path and the beam diameter:

$$W^2 > 8\gamma^2 \lambda_s l = 2\lambda_p l$$

and

$$l < \frac{c}{\omega_p} \sqrt{2\gamma} = \frac{4\pi\epsilon_0 \gamma^3 m c^3 \lambda_s}{eI} \quad (12)$$

These conditions constitute severe constraints; it is not possible to achieve an arbitrary beam monochromaticity without either reducing the beam current or eliminating the momentum spread due to space charge. In the example discussed above, reducing the current for fixed n_e would force the beam diameter to become smaller than the waists of the optical fields assumed to be present in the resonator. On the other hand, if means of removing the space-charge induced momentum spread can be found, Equations 2, 10, and 12 would no longer apply and $\Delta P_z/P_z$ would become an adjustable parameter.

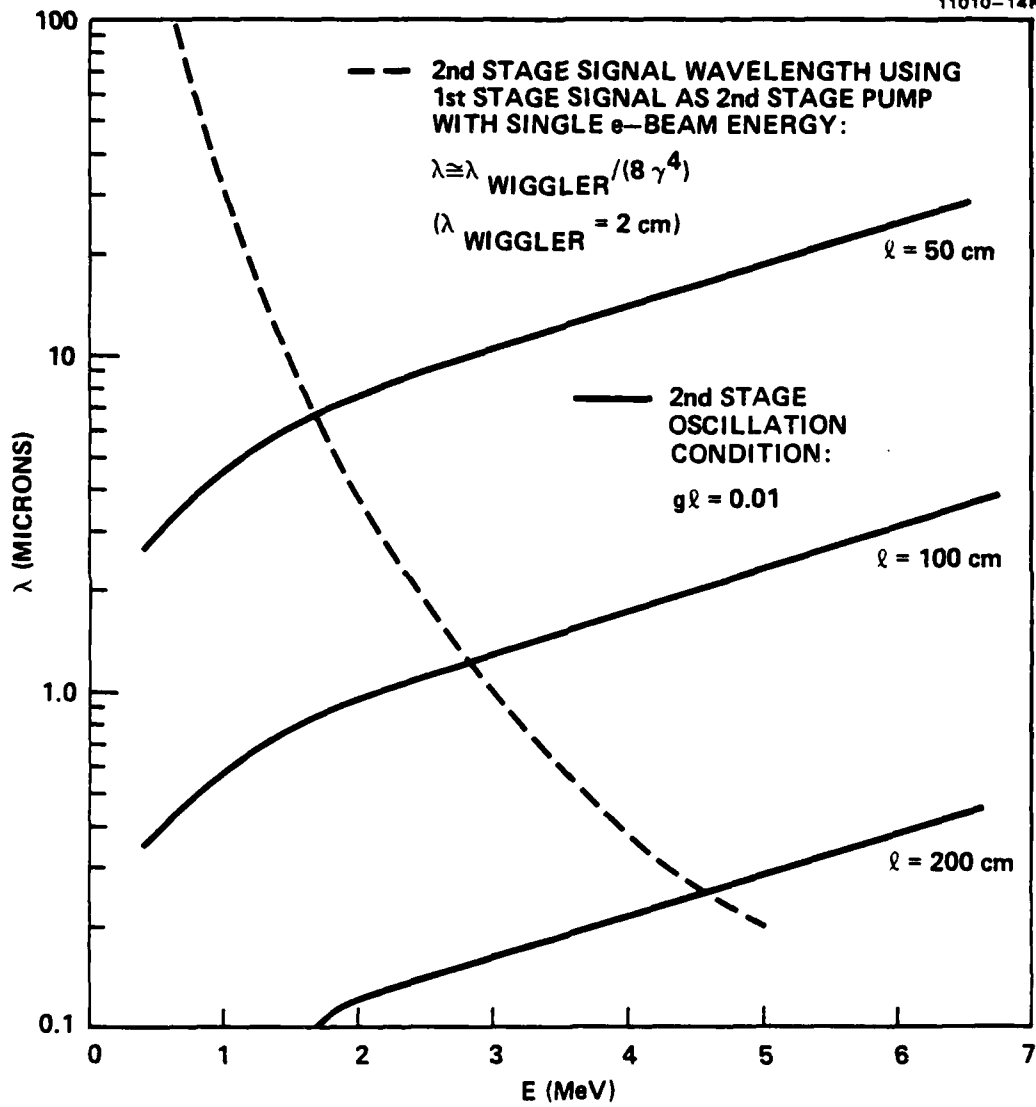


Figure 3. Oscillation conditions for a two-stage FEL.

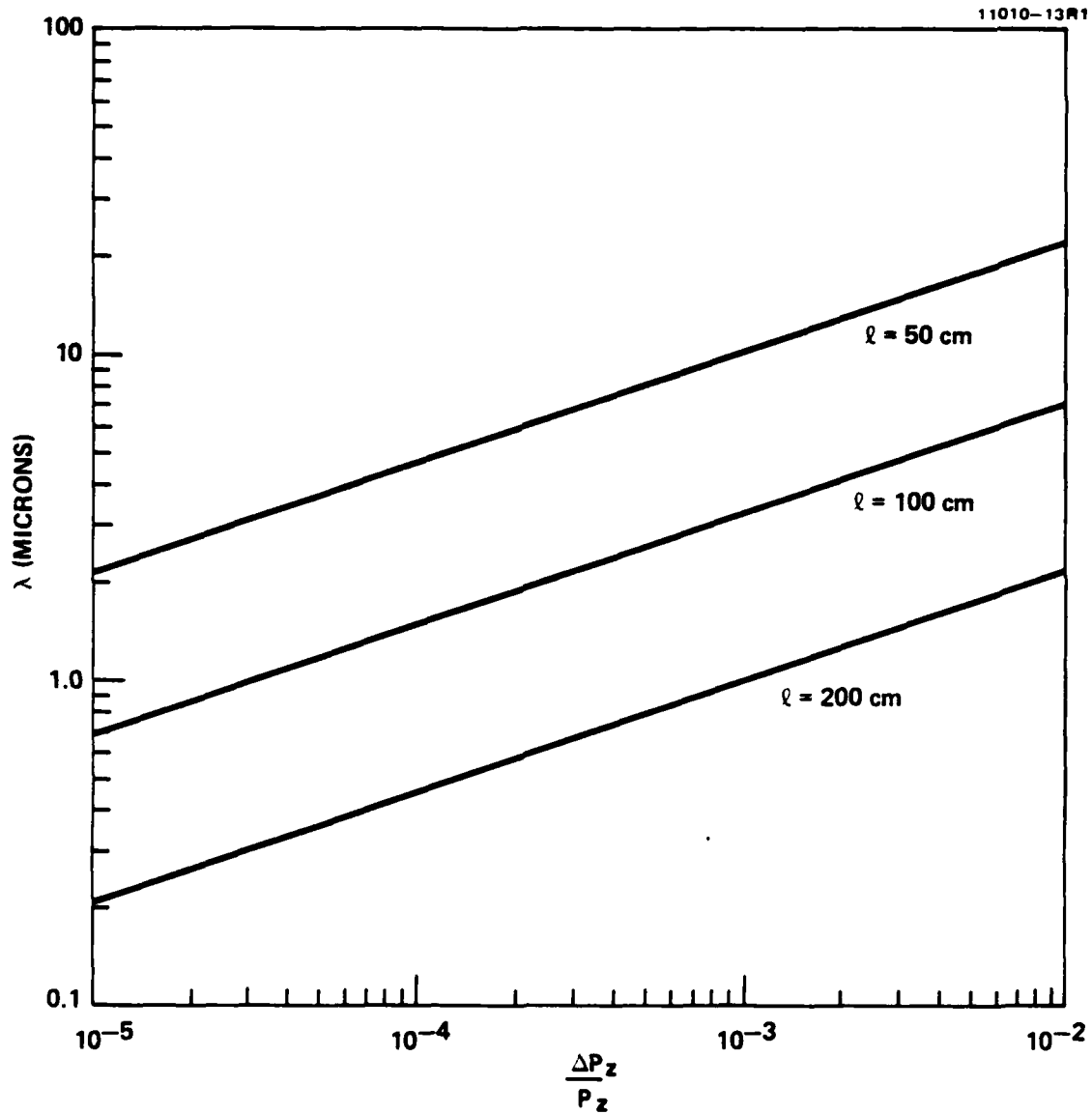


Figure 4. Electron beam monochromaticity requirement for Figure 3 oscillation condition.

SECTION 3

ELECTRON GUN AND COLLECTOR DESIGN

A. ELECTRON GUN

Critical to the operation of a practical two-stage FEL is an e-beam with a small longitudinal momentum spread. A hot-cathode e-gun has been chosen as a source for the e-beam. The preference for the hot-cathode gun is due to the low energy spread and low temperature with which the electrons are emitted at the cathode surface. Other systems operating with field emission guns generate electrons with a much larger energy spread at the emitting surface and, therefore, are less suitable to FEL use, or are not capable of cw operation.

The baseline hot-cathode e-gun has a Pierce-type, non-gridded geometry. Numerical simulation of the design parameters for the e-gun have been obtained using the relativistic Electron Trajectory Program written by W.B. Herrmannsfeldt.⁵ Variations of electrode shape and position were carried out until a laminar beam was obtained. Typical computer-plotted trajectories in the e-gun and equipotential lines are shown in Figure 5. The output data of the Electron Trajectory Program are then used as inputs for Brillouin flow calculations or as comparisons for future Electron Trajectory Program runs. The baseline e-gun design parameters are given in Table 1.

Table 1. Baseline E-Gun Design Parameters

Cathode Radius	2.013 cm
Cathode Curvature	14.46 cm
Overall Length	12.46 cm
Voltage	4×10^5 V
Current	38.42 A
E-Beam Radius on Exit	0.698 cm
$\Delta\phi$ (Unbiased Cathode)	1350 V

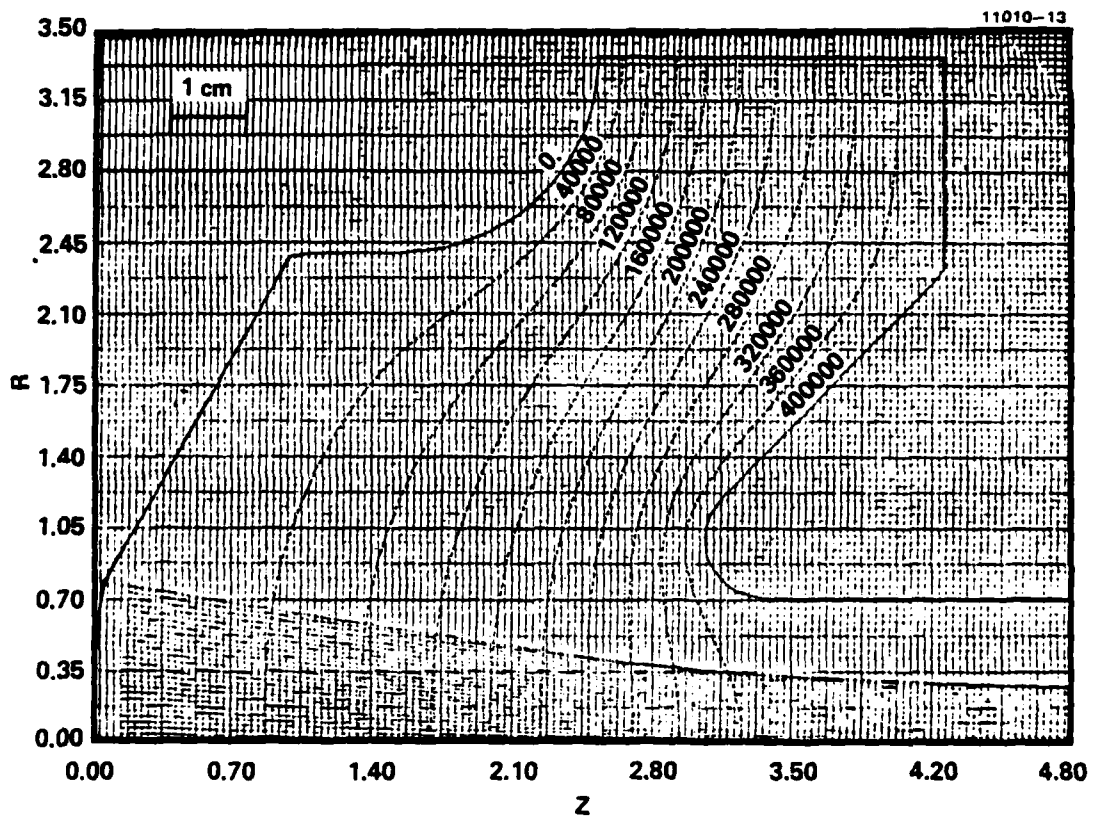


Figure 5. Typical computer plot of the electron trajectories and equipotential lines in the e-gun.

B. BRILLOUIN FLOW

The e-beam is injected into an axial magnetic field to achieve two purposes. First, it prevents the spreading of the e-beam due to the space-charge forces. Second, the longitudinal momentum shear can be reduced using Brillouin flow by injecting the e-beam into a guiding magnetic field. As shown in Figure 2c, the solenoid entrance is placed so that the field does not penetrate the e-gun. This allows independent optimization of the e-gun and the magnetic field. Upon entering the field region, the electrons see an azimuthal impulse due to the strong radial magnetic field. The e-beam then initiates a rotation around the z axis. Under the ideal Brillouin flow conditions,⁶ the longitudinal momentum shear (generated in the e-gun because of the space charge effect) is cancelled, and is replaced by an azimuthal one. The azimuthal momentum is given as a function of the radial position in the e-beam by

$$P_{\theta}(r) = \frac{e B_{z0} r}{2} \quad (13)$$

The value of the guiding magnetic field, B_{z0} , required for Brillouin flow in a beam of radius r_b is

$$B_{z0}^2 = \frac{2 I m}{\pi \epsilon_0 c \gamma \beta |e| r_b^2} \quad (14)$$

The suppression of the longitudinal momentum shear has been achieved at the expense of the azimuthal one. It has been shown that the trade is a good one. In fact, in Reference 7, the effect of the azimuthal momentum shear on the FEL small-signal gain was proven to be small for e-beam currents smaller than 700 A for most cases of practical interest.

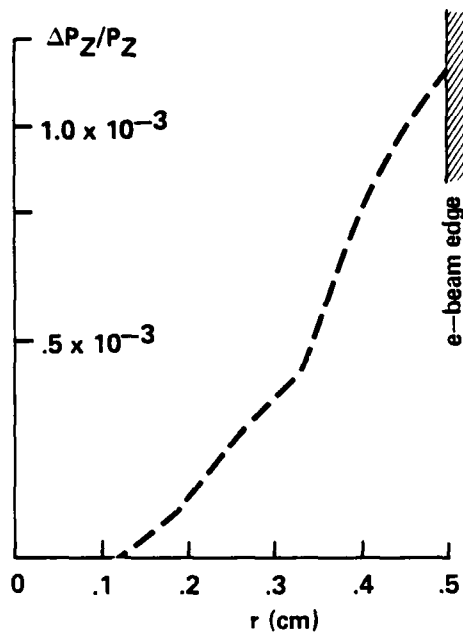
For conditions of the baseline e-gun the magnetic field requirement is $B_{z0} = 263$ G. The relation in Equation (14) is valid for $1 \ll \gamma < \infty$, it vanishes as $\gamma \rightarrow \infty$. The required guiding-magnetic field for extremely relativistic e-beams approaches zero because the poloidal self-magnetic field of the beam balances almost exactly the space-charge effects in the beam itself.

Numerical simulation of Brillouin flow has been carried out using the THERMR program⁸. This analysis indicates that the actual beam will follow a scalloped trajectory in the magnetic field. The height of the scallops is dependent on proper matching of the trajectories to the Brillouin field. The matching conditions for the baseline e-gun are shown in Table 2. Here, a somewhat higher value for the magnetic field B_{zm} is indicated than the value B_{z0} which was obtained by assuming a uniform beam profile and a larger radius.

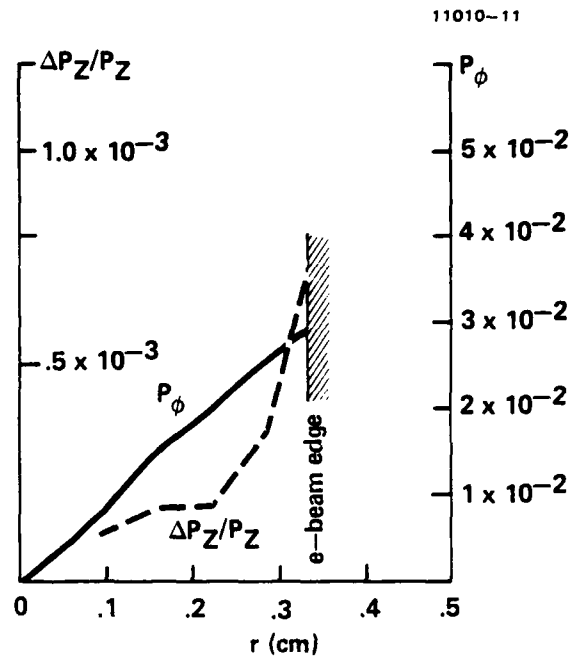
Table 2. Matching Conditions for the Baseline E-Gun

E-beam radius in the drift region	0.5336 cm
Scallop height	0.006 cm
Guiding magnetic field (B_{zm})	355 G
Pole piece radius (a)	4.572 cm

In Figure 6(a) $\Delta P_z/P_z = [P_z(r) - P_z(0)]/P_z(0)$ is plotted as a function of the radial position in the e-beam at the gun exit. In Figure 6(b) plots of $\Delta P_z/P_z$ and P_ϕ in the drift region are presented. We observe that the maximum value of $\Delta P_z/P_z$ has decreased in magnitude as expected. However, it did not achieve the ideal Brillouin condition which calls for $\Delta P_z(r)/P_z = 0$ for arbitrary value of the radius r . Combined with the diminishing longitudinal shear there is the onset of the azimuthal shear P_ϕ . Note the quasi-linear dependence of P_ϕ on r . This is consistent with the Brillouin flow model which requires the e-beam to rotate as a solid body. The residual $\Delta P_z/P_z$ in the drift region is due to the finite perveance of the e-gun and nonuniformity of the beam prior to entering the guide field.



(a) MOMENTUM SPREAD OF THE ELECTRONS AT THE E-GUN EXIT.



(b) MOMENTUM SPREAD OF THE ELECTRONS AFTER INJECTION INTO A BRILLOUIN FLOW GUIDE FIELD.

11010-11

C. SEGMENTED CATHODE APPROACH

Control of the axial-momentum distribution as a function of radial position can also be accomplished by biasing the cathode as illustrated in Figure 2(b). Concentric rings or segments of the cathode are biased at different potentials to offset the potential variation caused by the e-beam. Segments were introduced into the Electron Trajectory Program⁵ to determine the effectiveness of this technique. A typical plot of the momentum spread as a function of radial position is shown in Figure 7 for a 400 keV e-gun. Seven segments have been used for this case. As the number of segments is increased, a better potential match is possible and the maximum spread across the diameter of the beam is reduced to about 2.5×10^{-4} . The ideal match is obtained with a cathode potential which increases quadratically with radius. Segmented cathodes can approach this limit; but edge effects at the segment interfaces were not tested in the code due to the finite grid size; hence the momentum spread may be limited in practice by engineering constraints on the structure of the cathode segments.

D. THERMAL EFFECTS ON PROPAGATION

A numerical simulation of the thermal effects has been performed to trace electron trajectories from the unsegmented cathode surface into the downstream drift region. At each point on the surface of the cathode, a bundle of thermal electrons is emitted mostly in a cone of semiangle $\delta\alpha = (kT_c/e\phi)$ with the cone axis normal to the surface of the cathode. Here k is Boltzman's constant, T_c is the cathode temperature, e is the electron charge and ϕ is the potential. A computer run was performed in which each ray normal to the surface was replaced by two rays, each carrying half of the current of the original ray, and at an angle of $\pm\delta\alpha$ relative to the normal of the surface of the cathode. It was found that very little change occurs in the initial trajectories. This, however, is not the case when one propagates the beam in the drift region. If the beam is propagated too far, trajectory crossovers and cathode images occur. One must, therefore, not propagate the beam far enough to allow this to happen. The

THERMR program⁸ was used for the electron-trajectory analysis. This program plots the value of R_e , the radial displacement of an electron starting

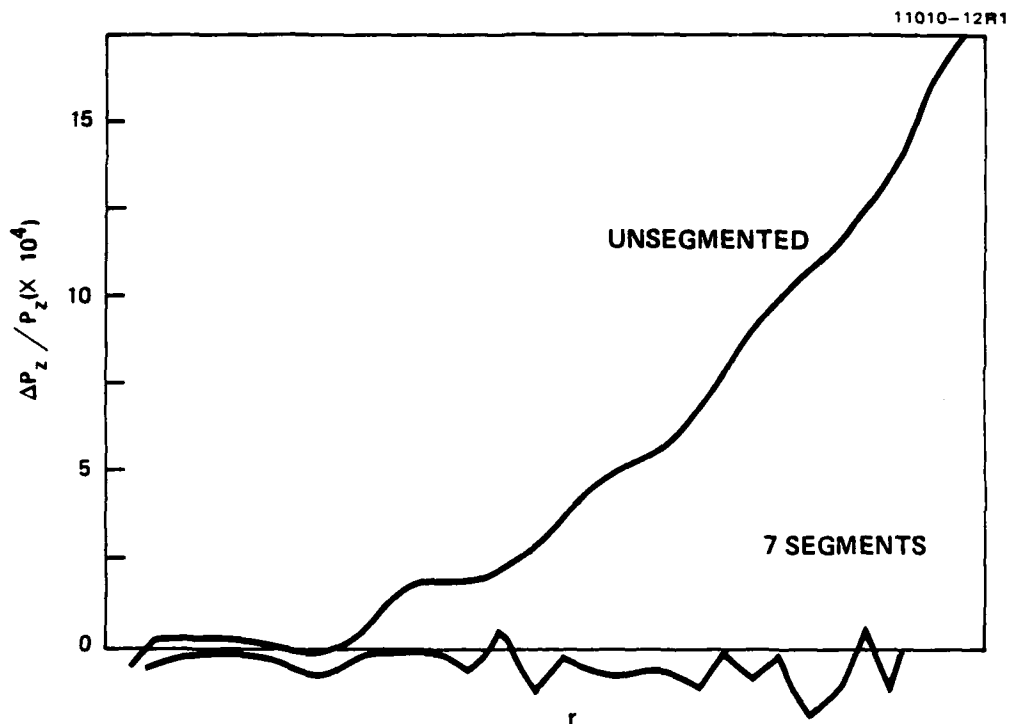


Figure 7. Momentum spread as a function of radial position for segmented and unsegmented cathodes.

from the edge of the cathode, and σ , the displacement of an electron starting on axis with transverse velocity kT/m . R_{95} is the radius which includes 95% of the electron beam. The ratio R_e/σ is a measure of the quality of the beam, for $R_e/\sigma > 3$ the beam retains a square cross-section while for $R_e/\sigma < 3$ it diffuses into a Gaussian shape. In Figure 8, σ , R_e and R_{95} have been plotted versus z , the distance from the cathode for the baseline e-gun. R_e/σ is greater than 3 for most of the drift region; therefore, no large dispersion of the beam is expected.

E. DEPRESSED COLLECTOR

Another critical component in a low voltage FEL is a depressed collector, which can efficiently recover the e-beam energy. Depressed collectors have been used in the past to improve the efficiency of traveling wave tubes and klystron devices.^{9,10} These collectors operate at near cathode potential. They use the formation of a negative space-charge depression (which is due to the slowing electrons), to inhibit the return of secondary and primary electrons to the anode. They normally operate with e-beams of a few tens of kilovolts and relatively large energy spread in the beam itself. Improvements in their efficiency was usually sought by increasing the number of stops held at different potentials to accommodate electrons with a wide range of energies.

The depressed collectors for a low voltage FEL must operate with e-beam energies of 10^5 to over 10^6 V, and with very small energy spreads, a few percent at most. It is possible, as will be shown later, to design efficient depressed collectors with very few stages, one stage will suffice most of the time. Particular attention, however, is required in designing the cup of the collector in such a way that a negative-potential gradient will be established at the surface of the cup to suppress the secondary-electron leakage current which could backstream and severely decrease the recovery efficiency.

The Electron Trajectory program⁵ was used to predict the performance of the depressed collector. Computer plots of the depressed collector are shown in Figures 9 and 10. The e-beam emerges from the drift region with a radius of 1.1 cm. It has been found that the depressed collector operates better if no magnetic field leaks into it. To this end, a pole piece of 1.5-cm radius has been placed at the end of the drift region. The high voltage electrode of the

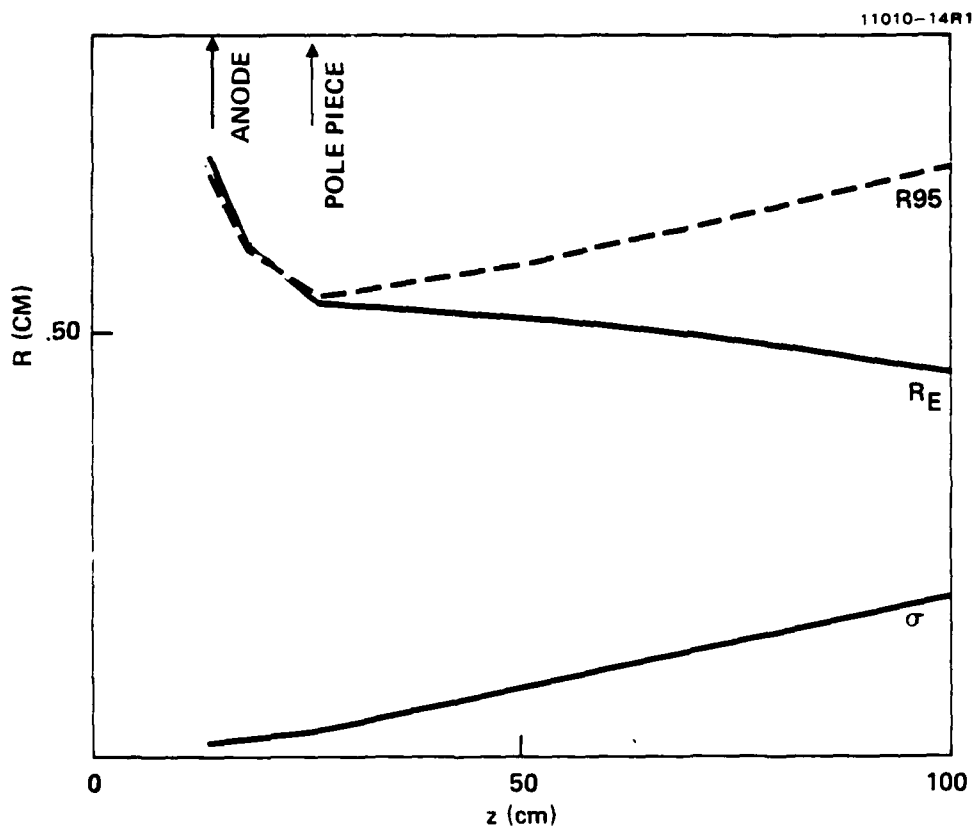


Figure 8. Relevant electron trajectory plot for the baseline e-gun.

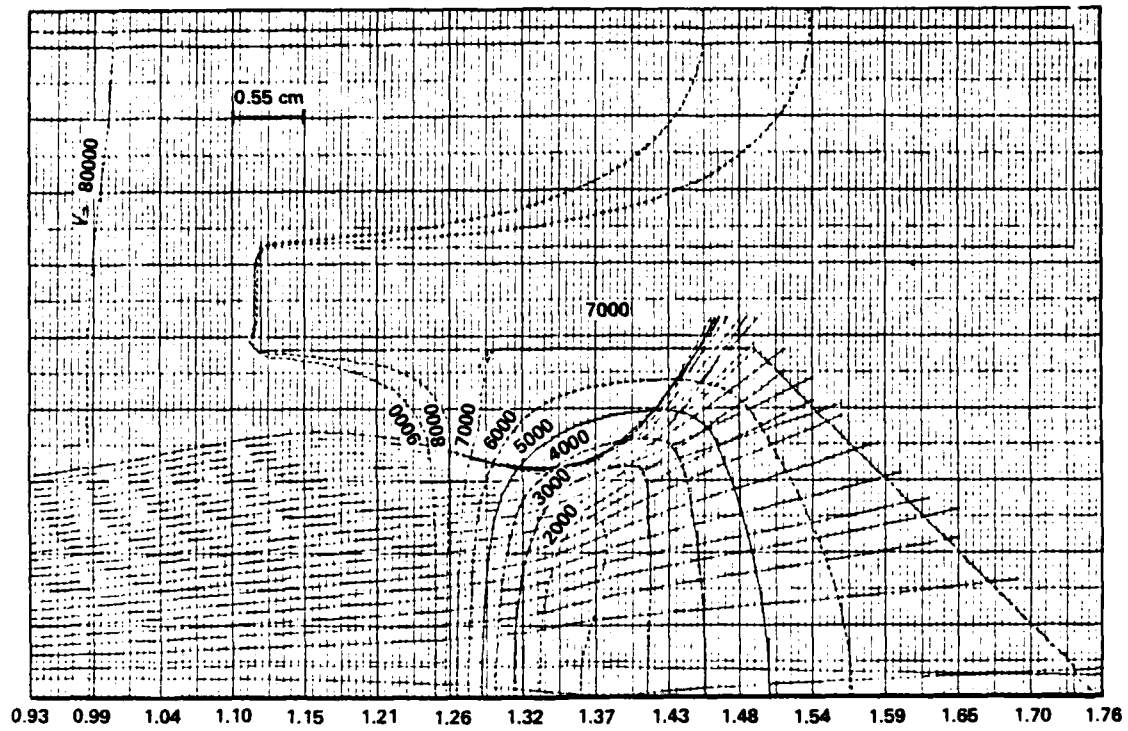


Figure 9. Computer plot of the equipotential lines and electron trajectories in the depressed collector. Depressed collector voltage is 7 kV.

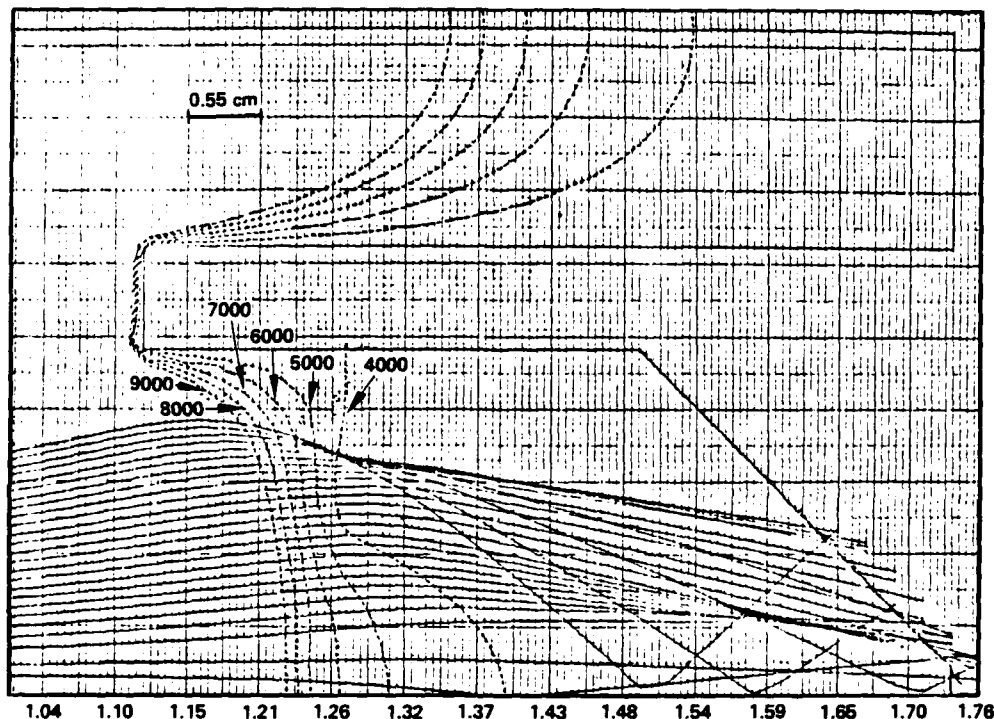


Figure 10. Computer plot of the equipotential lines and electron trajectors in the depressed collector. Depressed collector voltage is 4 kV.

depressed collector is 4.5 cm removed from the pole piece. This insures that the whole depressed collector is magnetic-field free.

Thermal effects generate a parabolic electron density distribution, $n(r)$, at the entrance of the depressed collector. We approximated this distribution by

$$n(r) = n_0(1 - r^2/r_b^2) \quad . \quad (15)$$

Where the constants n_0 and r_b were adjusted to match the beam density profile at the end of the drift region, i.e., $r_b = 1.1$ cm and $n_0 = 4.63 \times 10^9 \text{ cm}^{-3}$. The input data for the numerical calculations include the kinetic energy of the electrons as function of their position in the e-beam and the slope of the trajectories at the entrance of the depressed collector. The total energy of the electrons minus the rest mass can be chosen to be zero, without loss of generality, i.e.,

$$[\gamma(r) - 1] mc^2 - |e|\phi(r) = 0 \quad (16)$$

If ϕ is prescribed, γ can be computed and vice versa from Equation (16). Neither ϕ or γ are, however, known a priori; ϕ , in fact depends on the space-charge distribution inside the e-beam and the geometry of the depressed collector. An iterative procedure has been used to consistently compute ϕ and γ .

Initially we set $\phi = \phi_0(r)$, where $\phi_0(r)$ is the potential distribution inside an infinitely long cylindrical e-beam of constant radius with $n(r)$ given by Equation (15). Using the Poisson equation, we find

$$\phi_0(r) = \phi_p - \frac{3}{16} \frac{e n_0}{\epsilon_0} r_b^2 \left[1 + \frac{4}{3} \ln(r_p/r_b) \right] + \frac{e n_0 r^2}{4 \epsilon_0} (1 - r^2/4r_b^2) \quad (17)$$

where r_p is the radius of the cylindrical metal enclosure of the e-beam.

Substituting $\phi = \phi_0$ into Equation (16), we can compute γ_0 which can be used for the first run of the Electron Trajectory Program. From the potential map of the output of the Electron Trajectory Program, a new approximation $\phi_1(r)$ can be obtained at the entrance of the depressed collector. From Equation (16) a new set of values of $\gamma_1(r)$ is obtained and a new run of the Electron Trajectory Program performed. The iteration procedure converges rapidly.

The numerical simulation has been performed using a 400 keV beam energy and varying the cup potential V_{dc} from 7000 to 2000 V with decrements of 1000 V. The results for cup potentials of 7000 V and 4000 V are shown in Figures 9 and 10. In Figure 9 the equipotential lines clearly show the space-charge generated potential well in the center of the depressed collector cup. The negative potential gradient generated by the space-charge depression effectively suppresses any secondary emission current. We, therefore, can expect that the whole e-beam can be collected at 7000 V.

A reduction of V_{dc} to 4000 V caused the e-beam to pinch and a positive potential gradient is established on the surface of the collector. All the beam electrons are capable of reaching the surface of the collector but the unsuppressed secondary emission current may not allow the operation of the depressed collector at such a low voltage. The space-charge depression forms at between 4000-5000 V or about 1% of the beam voltage. It appears that operation with $V_{dc} > 4000-5000$ V would be feasible; this would imply a maximum recovery efficiency $\eta_r \approx 0.990 \sim 0.987$.

SECTION 4

ELECTRON BEAM MONOCHROMATICITY MEASUREMENT APPROACH

A. APPROACHES

Development of e-beams with low energy spread requires the measurement of the longitudinal velocity spread of the e-beam. Below we discuss approaches that we considered for this measurement and a detailed description of the Thomson scattering technique chosen for the measurement.

Several approaches to measuring the longitudinal-energy spread of the e-beam were studied in this program. Among the considered approaches were:

- (1) The use of beam energy analyzers: This method is not suitable for our purposes because it requires that the beam be dispersed. This disrupts the space-charge field of the beam which is the major source of energy spread one wants to measure.
- (2) Spectral measurements of FEL static wiggler or Cherenkov first stage signal gain: The homogeneous linewidth of the FEL gain is given by Equation (4). For a 400-keV beam this fractional linewidth is 4×10^{-2} which is much greater than the inhomogeneous linewidth due to the fractional energy spread (10^{-4}) of the beam. The Cherenkov generator also has too large a homogeneous linewidth.¹¹ Thus, this method has inadequate resolution to measure the beam monochromaticities of interest.
- (3) Side-looking Thomson scattering: Thomson scattering is a well-known technique for measuring the electron distribution in a moderately dense plasma. For the low-electron densities present in the FEL electron beam the major difficulty in using this technique is to obtain a sufficient signal-to-noise figure in the detected-scattered radiation. For an angle of incidence of the scattering beam $>10^\circ$ from the backward direction of the scattered beam (even for a high power incident CO₂ laser), the intensity of the scattered beam is too small to perform the spectral measurements required to resolve a 10^{-4} energy spread on the e-beam. Also, for the e-beam energies used in the present study (~400 keV) the electron velocity is not quite large enough to Doppler shift an incident 10.6- μm CO₂ laser wavelength into the wavelength range ($<1 \mu\text{m}$) where high sensitivity detectors can be used to detect the scattered radiation.

PRECEDING PAGE BLANK-NOT FILLED

- (4) Delayed scattering: Delayed scattering is an untried coherent scattering technique where a Neodymium:YAG laser (1.06 μm) is added to the side-on Thomson scattering equipment and the CO_2 beam is made coaxial to the e-beam. The resulting laser interaction pre-bunches the e-beam, which coherently scatters and up-shifts the CO_2 beam at the 1.06 μm wavelength. The scattering takes place downstream from the YAG laser beam and the intensity may be shown to have a Bessel function envelope in space which is modified by the thermal-velocity distribution of the electrons. While this technique may prove relevant to FELs, it is judged too complicated to be a reliable measure of the e-beam energy spread.
- (5) Back-scattered (end-on) Thomson scattering: Back-scattered Thomson scattering is the method selected for measuring the e-beam monochromaticity. Reducing the angle of both the incident and scattered radiation to near zero not only increases the back-scattered intensity due to the relativistic-beaming effect but also increases the Doppler shift to the point where the scattered 10.6- μm radiation is in a wavelength range where high sensitivity detectors are available.

B. THOMSON SCATTERING FROM AN ELECTRON BEAM

Thomson scattering is a conventional technique used to measure the thermal-energy distribution of plasmas. Here we apply it to the measurement of the energy spread in an e-beam. The experimental layout is shown in Figure 11. The classical relationship of the scattered wave vector, k_s , and incident wave vector, k_i to the electron velocity, v , and the respective frequencies is given by

$$(k_s - k_i) \cdot v = \Delta k \cdot v = \Delta\omega = \omega_s - \omega_i \quad . \quad (19)$$

By measuring the frequency shift $\Delta\omega$ as a function of the various angles, one can in principle find the velocity distribution of the electrons. While the scattered intensity from a typical electron density of $n = 10^{10} \text{ cm}^{-3}$ would be low in the rest frame (RF) of the electrons, several features of the relativistic-scattering process significantly enhance the effective scattered intensity.

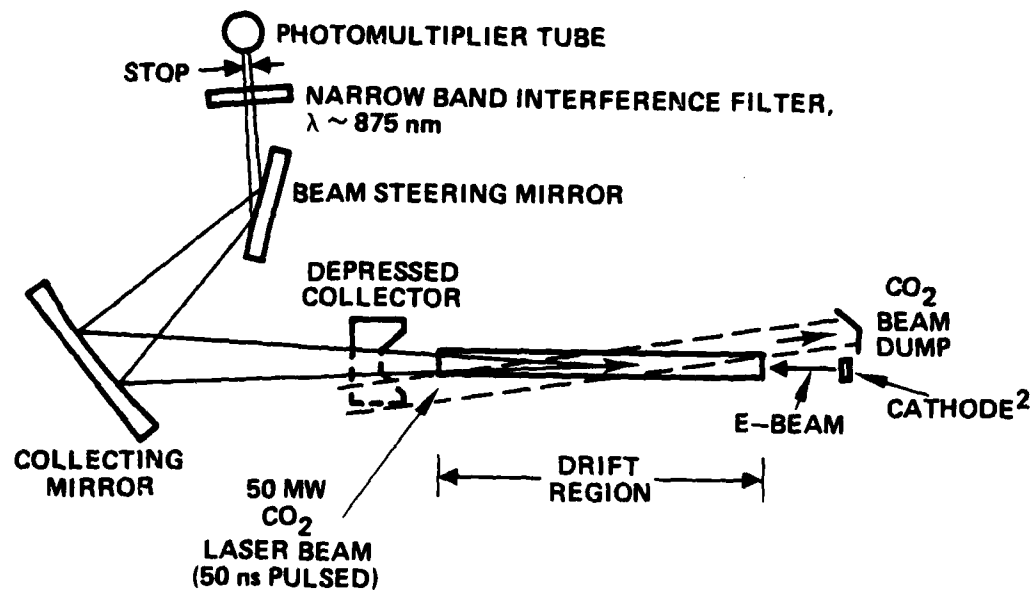


Figure 11. Experimental layout of the Thomson scattering experiment.

First, the incident plane wave is Doppler shifted as it is transformed from the laboratory reference frame (LF) to the (RF). This increases the frequency (photon energy) and the intensity (photon energy times counting rate) as the wave opposes the e-beam. In the RF, the incident Doppler-enhanced intensity is scattered classically, yielding a dipole-radiation wave which falls off quadratically with radius. Upon transforming back to the LF the "reflected" dipole wave is enhanced again in frequency and intensity due to a second Doppler shift. In addition, the Lorentz transformation of the angles collapses the dipole pattern towards the axis of the beam further enhancing the intensity.

The net result is an increase of about three orders of magnitude due to relativistic effects at voltages on the order of 400 keV. Finally, by passing the probe beam axially down the e-beam (as shown in Figure 11), and collecting the back-scattered light, the total number of electrons involved in the process are maximized. The small scattered intensity is within the range of existing diagnostic equipment. The frequency shifts are on the order of 10 times, making a CO₂ laser practical as a probe beam source.

1. Polarization

In our case we are interested in measuring the longitudinal energy of the electrons. This means we wish Δk to be parallel to the beam velocity v . This is a Lorentz invariant condition which is true in the RF as well as the LF. It defines a scattering plane as shown in Figure 12. Also shown are the principal polarizations of the electric field, E , that are of interest. The electric field vectors lie in (\parallel) and out (\perp) of the scattering plane. The Thomson scattering cross sections are well known in the RF, and in the following discussion primed variables refer to the RF. The E_{\parallel} vector determines the direction of oscillation of the electrons and the alignment of the Thomson scattered dipole radiation. This radiation has a toroidal intensity profile given by

$$I'_{\parallel} = \epsilon_0 E'_{\parallel}{}^2 = N' \epsilon_0 E'_{\perp}{}^2 \cdot \frac{r_0^2}{r'^2} \cos^2 \alpha'$$

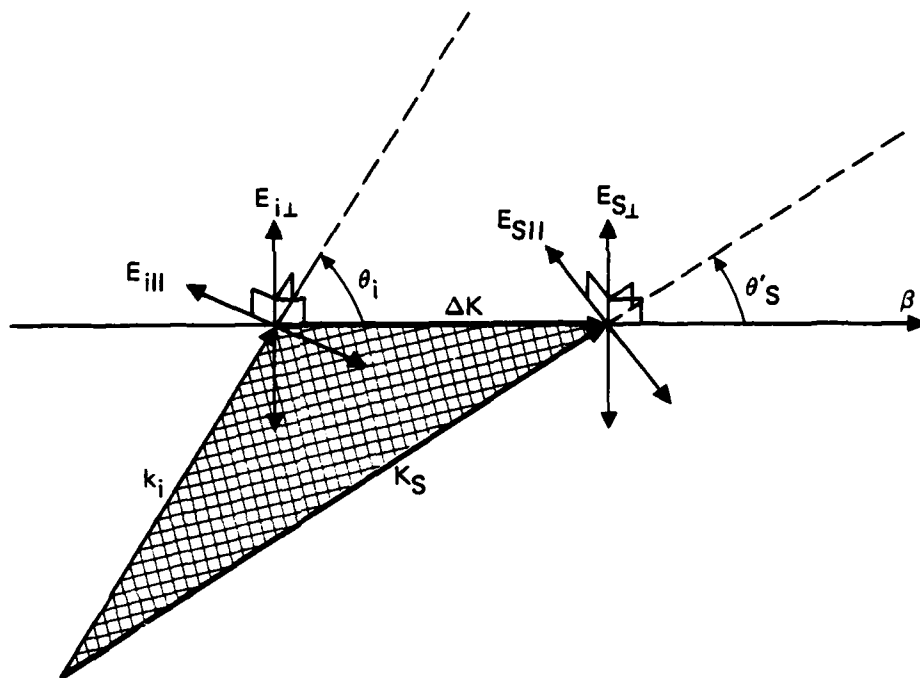


Figure 12. E-field and wave vectors for the Thomson scattering experiment.

as shown in Figure 13. Here, $r_0 = 2.83 \times 10^{-15}$ m is the classical electron radius, r' is the distance from an electron to the detector, and N' is the total number of electrons in the scattering volume. The preferred angular arrangement is to use the polarization with $\alpha = 0$. This is automatically obtained by backscattering.

2. Doppler Shifts and Energy Density Enhancement

McKinley¹² has derived the relativistic transformation of the solid angle by using photon conservation and has shown how this correction contributes to the light intensity received by fixed detectors from compact moving sources. McKinley's results can be confirmed by direct transformation of the incident and scattered Poynting's vectors. We have introduced below, an additional correction due to dipole polarization. Following McKinley's notation the characteristic Doppler shifts are given by

$$D_i = \gamma(1 - \beta \cos \theta_i) \quad (20)$$

and

$$D_s = \gamma(1 - \beta \cos \theta_s) \quad (21)$$

where θ is the angle between the wave vector and the e-beam in the LF for each of the scattered (s) and incident (i) waves.

The transformation from the LF to the RF for the frequencies ω' are given by:

$$\omega'_i = D_i \omega_i \quad (22)$$

and

$$\omega'_s = D_s \omega_s \quad (23)$$

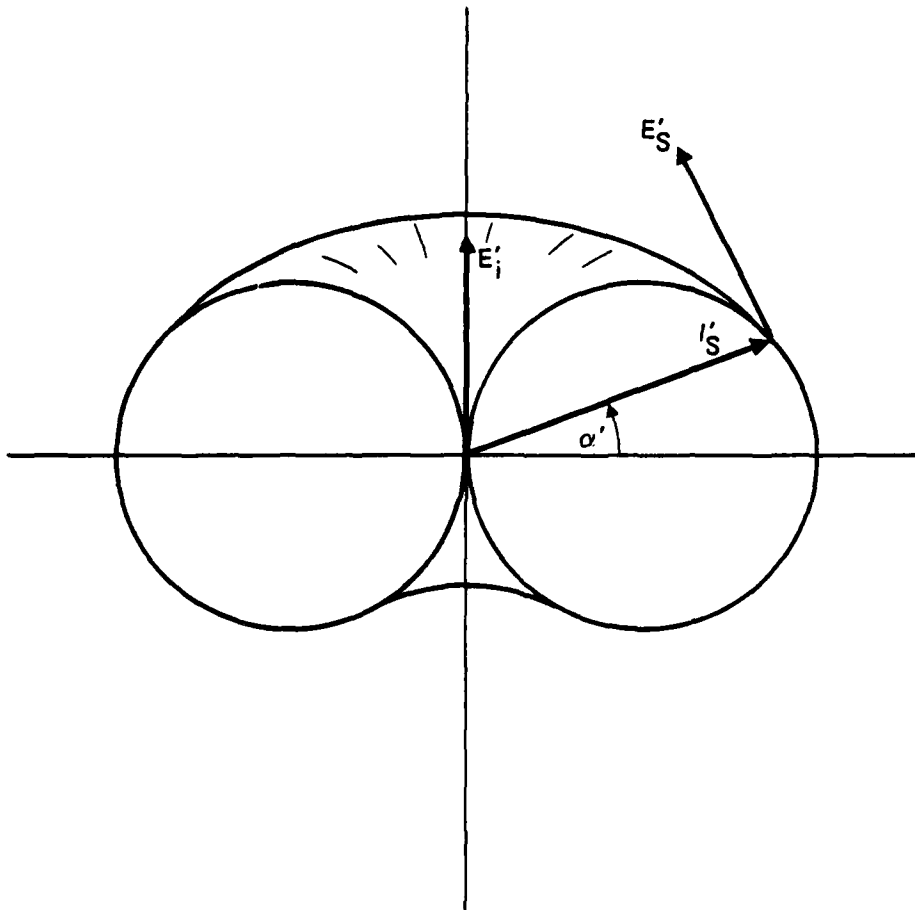


Figure 13. Thomson scattering intensity profile in the electron rest frame.

In the RF the photon energies are negligible compared to the rest mass of the electron and we may assume conventional Thomson scattering takes place with $\omega'_i = \omega'_s$. The transformation for the plane incident wave intensity, I'_i , is given by:

$$I'_i = D_i^2 I_i \quad (24)$$

The Thomson scattered intensity of the waves in the RF is given by:

$$I'_s = N' \frac{r_o^2}{r'^2} \cos^2(\alpha') I'_i \quad (25)$$

and the scattered dipole wave by

$$I'_s(r', \alpha) = D_s^4 \left(\frac{\cos \alpha - \beta}{1 - \beta \cos \alpha} \right)^{-2} I_s(r, \alpha) \quad (26)$$

Since the proper frames for the scattering volume and the electron density are not the same, N' transforms as $N' = N/\gamma^2$. In the LF the net result is

$$I_s = \left(\frac{\cos \alpha - \beta}{1 - \beta \cos \alpha} \right)^2 \frac{D_i^2}{D_s^4} I_i \frac{N}{\gamma^2} \left(\frac{r_o}{r} \right)^2 \quad (27)$$

and

$$\omega_s = \frac{D_i}{D_s} \omega_i \quad (28)$$

The intensity is a maximum in the back-scattering case where $\Theta_i = \pi$ and $\Theta_s = 0$. Taking the polarization angle $\alpha = 0$ yields

$$I_s = \frac{(1+\beta)^2}{\gamma^4(1-\beta)^4} I_i N \left(\frac{r_0}{r} \right)^2 = \frac{(1+\beta)^4}{(1-\beta)^2} I_i N \left(\frac{r_0}{r} \right)^2 \quad (29)$$

and

$$\omega_s = \frac{1+\beta}{1-\beta} \omega_i \quad (30)$$

At 400 keV, ($\beta = 0.828$), the intensity ratio becomes

$$I_s/I_i = 377 N \left(\frac{r_0}{r} \right)^2 \quad (31)$$

and the frequency shift ratio is $\omega_s/\omega_i = 10.60$.

The frequency shift also applies to wavelength dispersion in the original beam; e.g., a $\pm 15 \text{ \AA}$ wavelength uncertainty, typical of a CO_2 laser band, is reduced to $\pm 1.4 \text{ \AA}$.

The angular roll-off of the intensity has half widths of 16° and 11° in the two principal polarization directions, as shown in Figure 14.

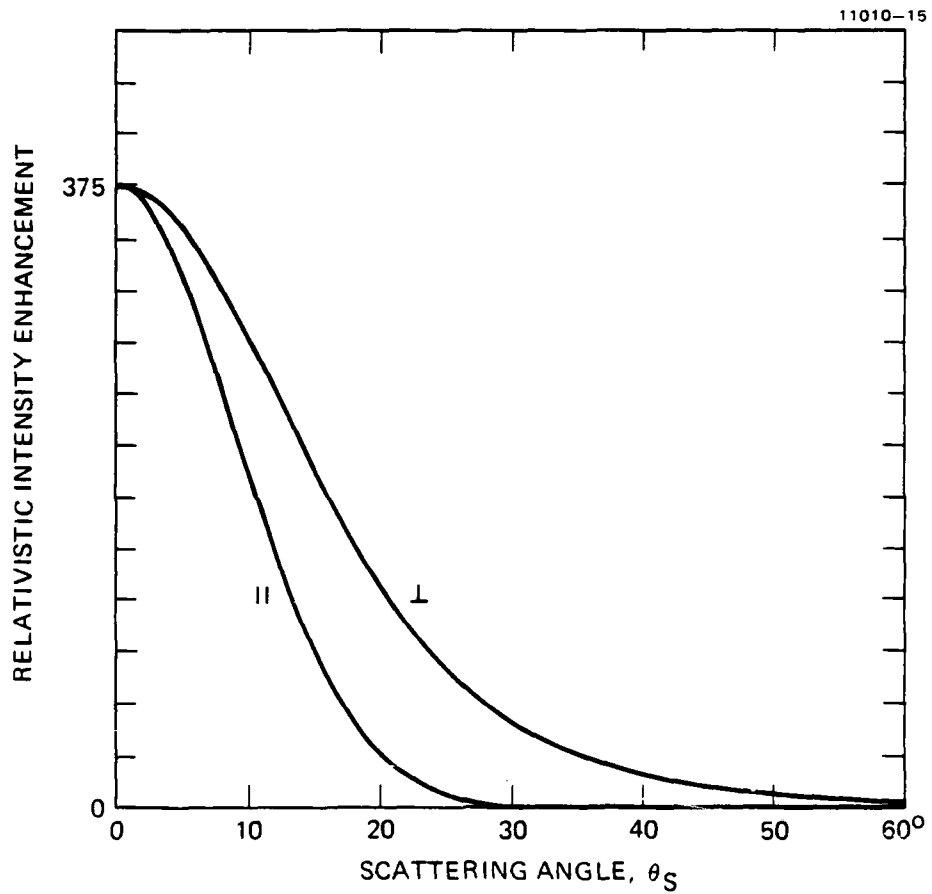


Figure 14. Relativistic intensity enhancement as a function of scattering angle.

Scattering Power

The axial scattered intensity with a 9.3- μm CO_2 laser intensity $I_i = 5 \times 10^{11} \text{ W/m}^2$, a scattering volume of $1 \text{ m} \times 10^{-4} \text{ m}^2$, and an electron density of 10^{16} m^{-3} (i.e., $N = 10^{12}$) is

$$\begin{aligned} I_s &= 377 N \left(\frac{r_0}{r} \right)^2 I_i \\ &= \frac{1.5 \times 10^{-3}}{r^2} (\text{W/m}^2) \end{aligned} \quad (32)$$

For an $f/20$ optical system (with $\theta_s < 3^\circ$, $f = r$ and an aperture of $D = 0.05 r$) the collected optical signal power, P , is found to be

$$P = \pi \left(\frac{D}{2} \right)^2 I_s = 3 \times 10^{-6} \text{ W} \quad (33)$$

or the equivalent of about 10^6 photons per pulse at 0.88 μm .

3. Frequency Shift Contributions

For general angles the scattering frequency is given by

$$\omega_s = \frac{1 - \beta \cdot k_i}{1 - \beta \cdot k_s} \omega_i \quad (34)$$

The variation of ω_s with β , k_i and k_s for the back-scattered case may be written for small angles as

$$\frac{\Delta\omega}{\omega} = 2\gamma^2 \Delta\beta_z - \frac{\beta_\theta \Delta\theta_s^2}{2(1-\beta_\theta)} + \frac{(\Delta\beta_\theta + \Delta\beta_r) \Delta\theta_s}{(1-\beta_\theta)} - \frac{\beta_\theta \Delta\theta_i^2}{2(1+\beta_\theta)} + \frac{(\Delta\beta_\theta + \Delta\beta_r) \Delta\theta_i}{1 + \beta_\theta} \quad (35)$$

The first term is the variation in frequency shift due to axial velocity fluctuations. It does not vanish with angle as do the remaining terms. The second and fourth terms, which are quadratic in the angles, are purely geometrical angular red shifts. The remaining terms are off-axis terms involving a coupling of the k vectors to the transverse velocity. The sign difference in the denominator makes the shift more sensitive to the scattering angle than incident angle. In the case of Brillouin flow, the large rotational velocity contribution $\Delta\beta_\theta$ must be suppressed by keeping $\Delta\theta < 1^\circ$.

While the frequency shift variations have been derived for Thomson scattering, they are also relevant to the design of the optical resonator. It is evident that all of these contributions may affect the gain bandwidth.

SECTION 5

SYSTEM MECHANICAL AND ELECTRICAL DESIGN

A. OVERALL SYSTEM

The overall system was designed around an existing vacuum chamber and 400-kV Marx-bank generator. The internal dimensions of the vacuum chamber are 183-cm long x 61-cm diameter. A photograph of the complete system is shown in Figure 15. The major components are: vacuum chamber, e-gun, solenoid, depressed collector, Marx-bank generator, CO₂ laser and control electronics. A system outline drawing is given in Figure 16. Shown here are each major component and its location. (The Marx-bank generator, and CO₂-TEA laser are inherently noisy devices, therefore precautions are taken to eliminate EMI from these sources). All control signals out of the screened room are on fiber-optic cables to eliminate noise transmitted back into the screened room. The screen room power has EMI filters. With these precautions and a tightly sealed screened room, noise is reduced to acceptable levels.

B. FEL COMPONENTS

The FEL components consist of the e-gun, solenoid and depressed collector. Photographs of these components are shown in Figure 17. Their mechanical design was in part dictated by the decision to operate the e-gun and depressed collector near ground potential.

The e-gun mechanical design evolved from the theoretical study outlined in Section 3, and the electrode shapes were modeled directly after the computer design profiles. The basic electrode shape is shown in Figure 5 of Section 3. The voltage standoff is accomplished by three 2.54-cm-diameter ceramic rods. This open style greatly reduced the cost of ceramics needed for this experimental gun. Heat shields are included on the output end of the anode to reduce heating of the end of the solenoid.

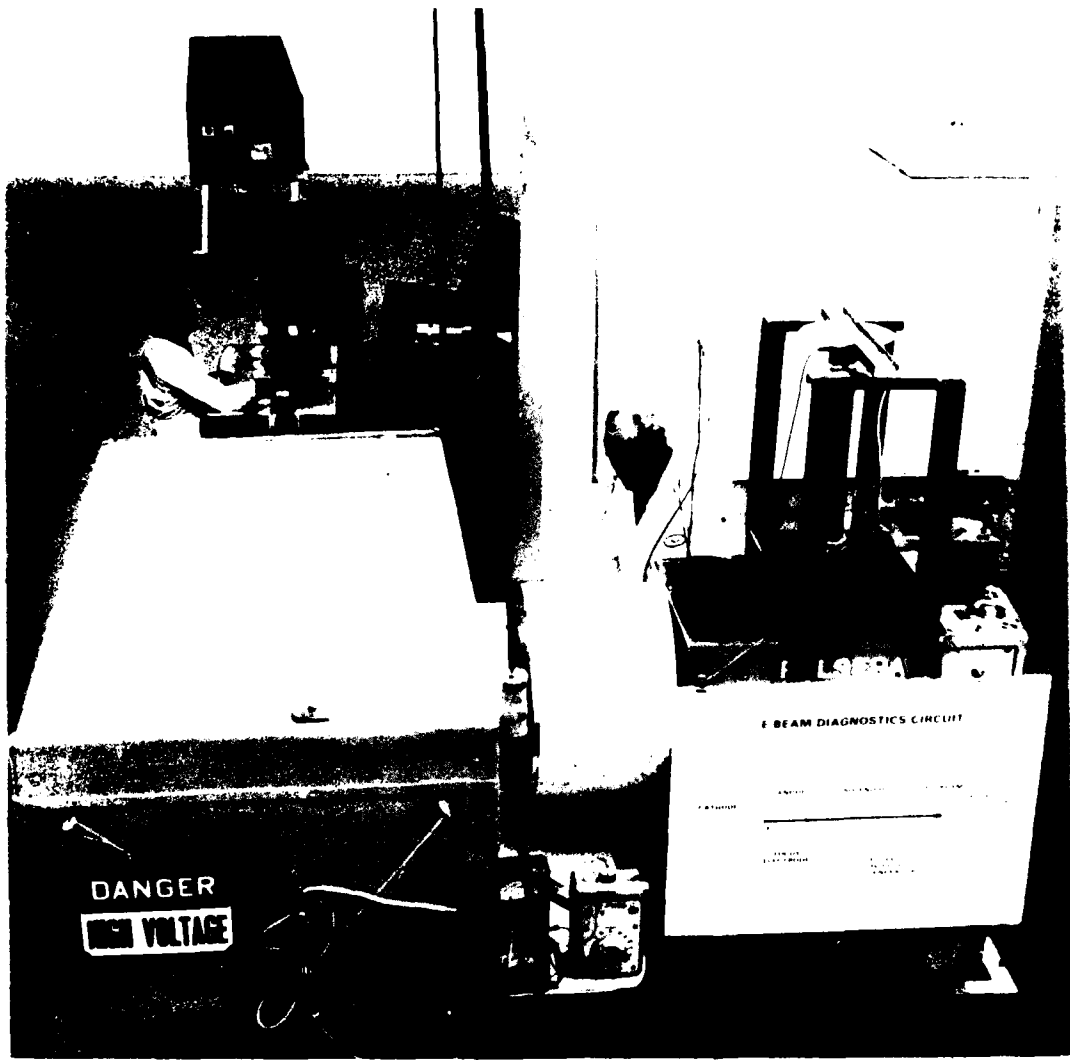


Figure 15. Hughes FEL experimental set-up.

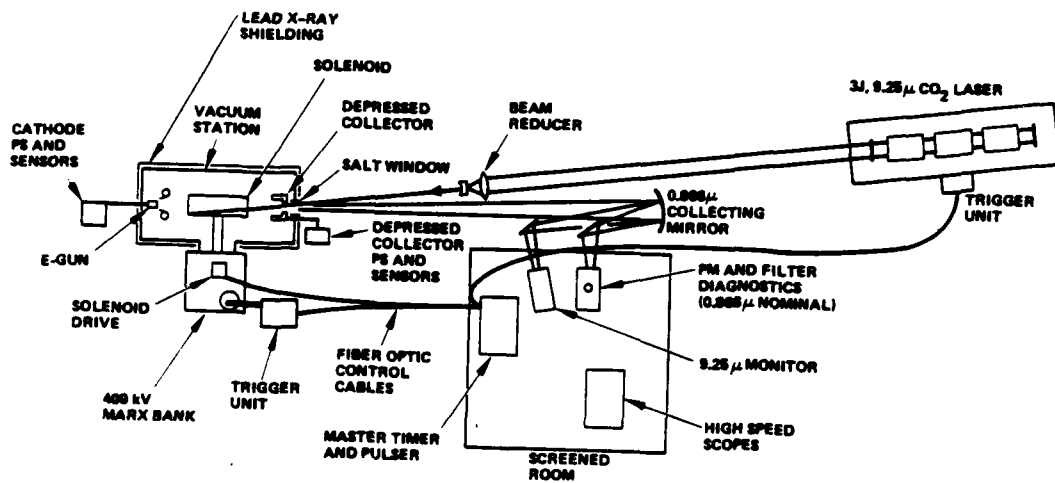
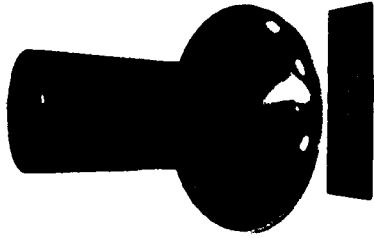
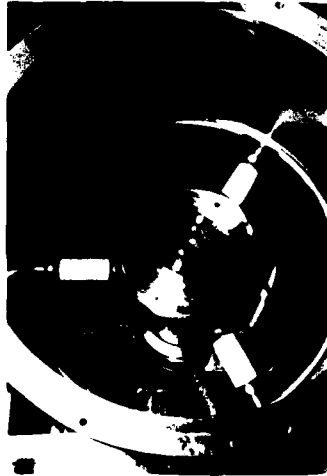
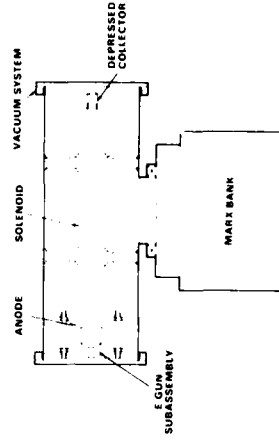


Figure 16. System outline drawing.

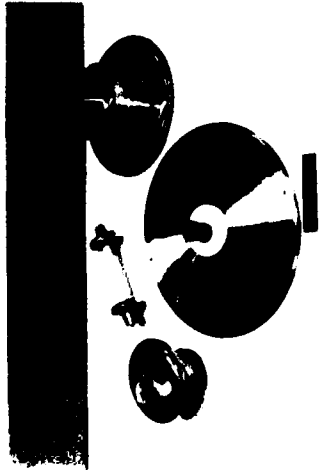
11010-8R1



DEPRESSED COLLECTOR



GUIDE FIELD



ELECTRON GUN



Figure 17. FEL components.

The solenoid is designed as an integral, sealed unit allowing the use of non-vacuum materials in its manufacture. The winding is made of six layers of 1-mm-diameter lacquer-coated copper wire, insulated layer to layer with Kapton film. It is operated in the pulsed mode by discharging a capacitor through the coil. The magnetic field in the solenoid rises to a peak of 400 G in 10 msec with 5.4-A of coil current.

The depressed collector has two basic components, the high voltage electrode on the end of the solenoid and the collecting cup (shown in Figure 18). As with the e-gun, it is shaped identically to the computer code profile of Section 3. A high voltage electrode is added to the solenoid with a spacing sufficient to ensure no magnetic field leaks into the collector (approximating a mirror image of the e-gun). This is important because secondary electrons will return on these field lines and reduce the collector efficiency. The shape of the collector cup yields a large open area while retaining the ability to form a space-charge well. During early phases of testing the e-gun, we replaced the depressed collector by a 10-cm diameter cathode-ray-tube screen assembly. This screen doubled as a crude depressed collector as well as a visual aid in monitoring the e-beam cross-section.

C. ELECTRONICS

The system electronics consists of a 400-kV Marx-bank generator, a solenoid driver, master trigger pulser, delay units, CO₂ discharge control circuitry, current and voltage sensors, optical diagnostics, and fiber optic control circuitry. A simplified diagram of the electronic diagnostic circuit is given in Figure 19.

The Marx-bank generator is an 8-stage device with an erected capacitance of 12.5 nF. The stored energy at 400 kV is 1 kJ. A 1-k Ω water resistor is placed in series with the anode to limit the current in the event of an arc. (Earlier experiments utilized a series inductor to round off the pulse rise at the anode; arcing at the anode tended to damage the inductor and it was replaced.)

The solenoid-driver circuit, shown in Figure 20, floats at 400 kV. It is battery powered and fiber-optically isolated. The solenoid driver circuit is essentially an overdamped LRC circuit, which is switched by an SCR. The capacitor is charged by a pulsewidth modulator which pulse charges the drive

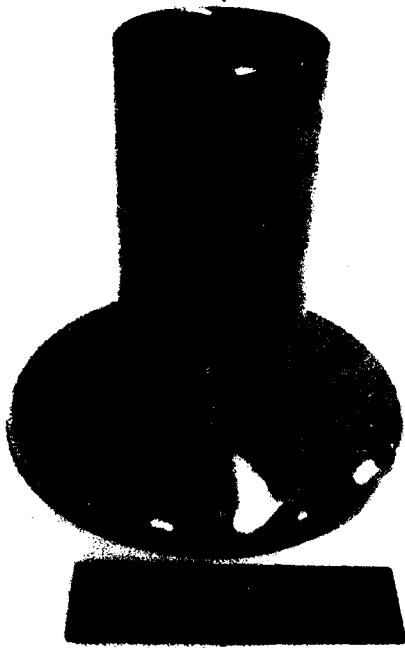


Figure 18. Depressed collector cup.

11599-5

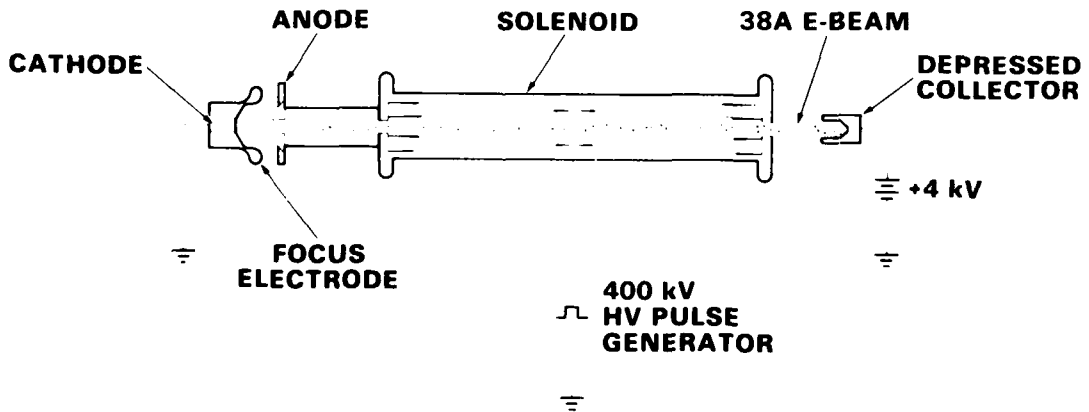


Figure 19. Electronic diagnostic circuit.

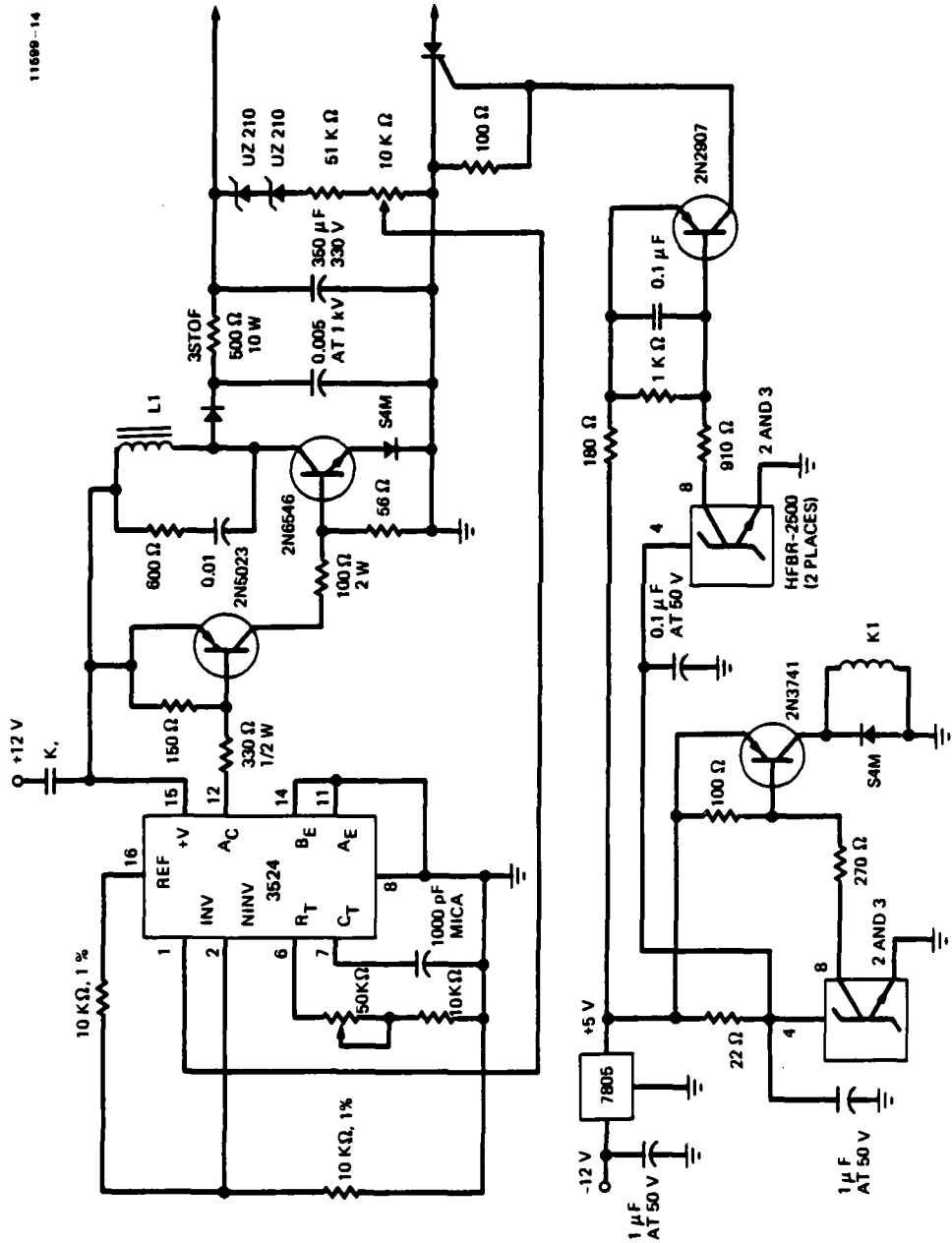


Figure 20. Solenoid driver circuit.

capacitor to 400 V. Power is provided by a 12 V, 20 A-h gell cell. The package fits in a box of dimensions 20 cm x 12 cm x 20 cm, which allows it to be mounted in the oil inside the Marx-generator tank. The circuit is remotely controlled ("start charge" and "pulse") and instrumented with fiber-optic relay circuitry which returns an analog current amplitude signal to the screened room.

The basic beam current sensors are Pearson Model 110 current transformers. One is mounted in the cathode ground circuit and monitors the e-gun emission current. The other is mounted in the high voltage leg of the depressed-collector circuit and measures the recovered beam current. An additional solenoid-current monitor is mounted inside the solenoid-driver box. It produces an analog light signal which is sent into the screened room and decoded as a measure of the solenoid current. With these three signals all information needed for depressed collector characterization can be obtained.

The control electronics consists of a series of timers, delay units and driver circuitry necessary to generate and time all of the pulses needed for circuit triggering. The pulse timing diagram is shown in Figure 21. The AC sync pulse allows firing of the Marx generator at the zero crossing of the filament current so that no filament-induced B field is present at the cathode during the "beam on" condition. All signals, including one used to fire the CO₂ laser during Thomson scattering experiments, are timed from a single "fire" button. The circuitry used to generate these signals is shown in Figure 22. All of the timing signals that are sent out of the screen room are first converted to light pulse signals; these signals are carried by fiber optic cables to the Marx bank, solenoid, and CO₂ laser trigger pulsers.

D. THOMSON SCATTERING

The mechanical set-up of the Thomson scattering experiment was shown earlier in Figure 16. The CO₂ laser 9.25- μ m output pulse is sent through a beam reducer which reduces its area to 1 cm² and recollimates the beam. A NaCl window is used to pass the beam into the vacuum chamber at an angle of 1°. A hole in the depressed collector is used to pass the probe beam into the solenoid and to view the scattered radiation. A 40-cm diameter, $r = 6$ m collecting

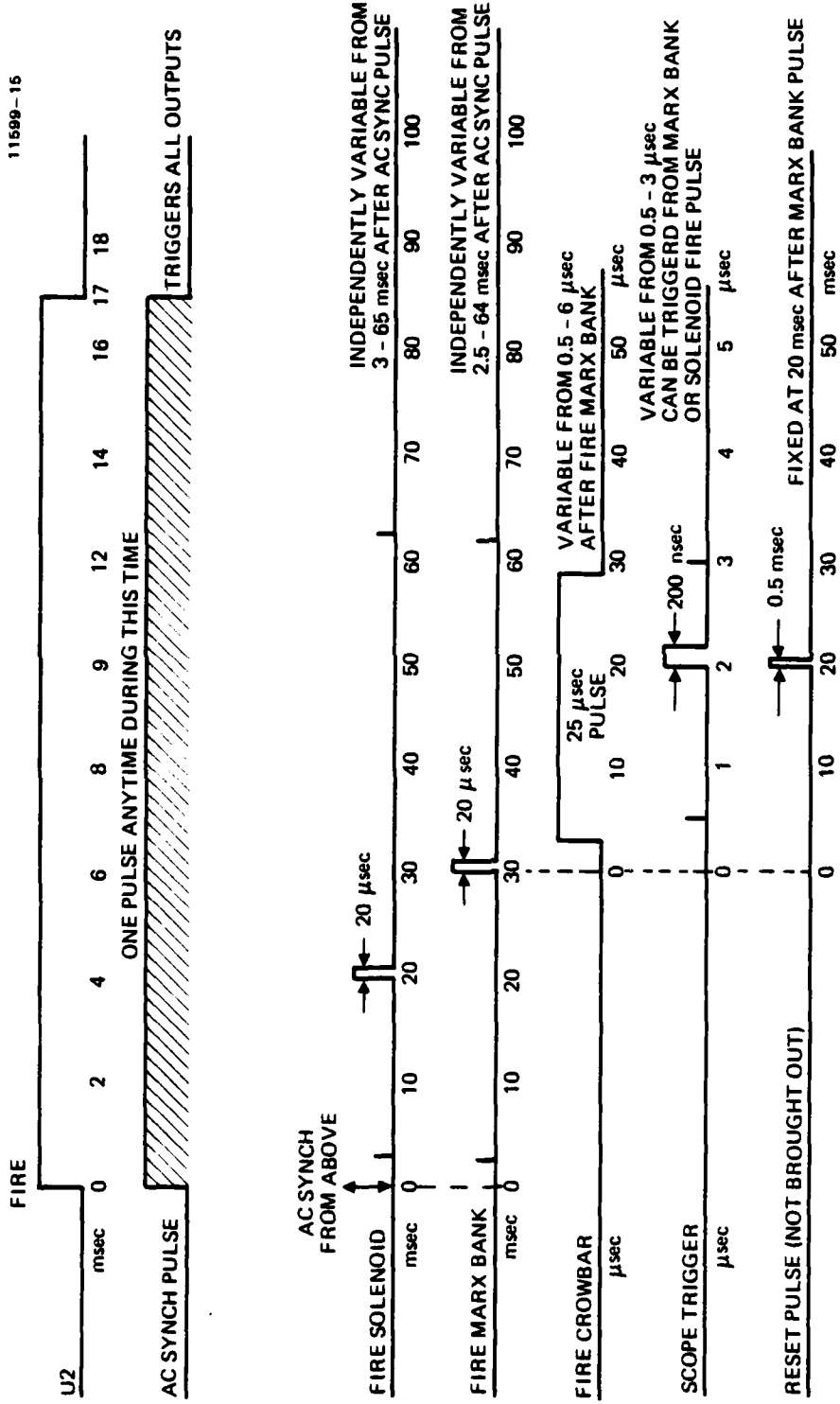


Figure 21. Pulse timing diagram.

mirror is aligned with the e-beam on axis and, with a second planar mirror, directs the scattered radiation into an S-20 side-on photomultiplier tube located inside the screened room. The temporal shape of the laser pulse is obtained by collecting the reflection off the salt window and directing it into a Ge detector. The nonideal scattering volume, optical surfaces and detector quantum efficiency will combine to reduce the total number of measured photons from that predicted in Section 4 by two to three orders of magnitude (or 10^3 per pulse).

SECTION 6
EXPERIMENTAL RESULTS

The experimental program has developed along four distinct but interrelated lines. These are vacuum chamber, e-gun, depressed collector and Thomson scattering. Each will be dealt with individually.

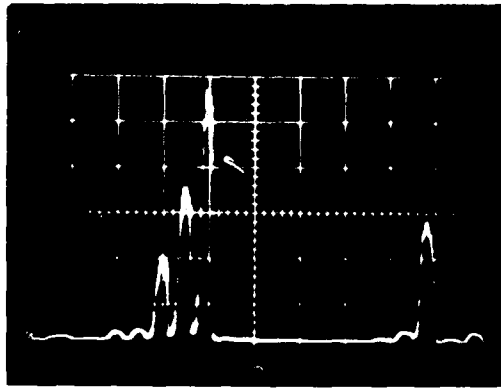
A. VACUUM CHAMBER

The vacuum chamber has a base pressure $P_0 < 2 \times 10^{-7}$ Torr. Operation of the e-gun for over 6 hr raises the pressure to approximately 4×10^{-7} Torr, due to radiative heating of the nearby surfaces. Published data on cathode performance¹³ indicates that pressures less than 5×10^{-6} Torr should be sufficient to allow long-time cathode operation at over 3 A/cm^2 . Our initial cathodes, however, never operated up to this expectation and some poisoning agent was suspected to be present. A UTHE gas-mass analyzer was installed to determine which poisoning substances were present. The mass analyzer was operated both with and without the e-gun in operation. Typical mass analyzer data is shown in Figure 23. Peaks, typical of helium, nitrogen, CO_2 , water and hydrocarbons could be seen out to $M = 149$, but no unusual poisoning agent was identified.

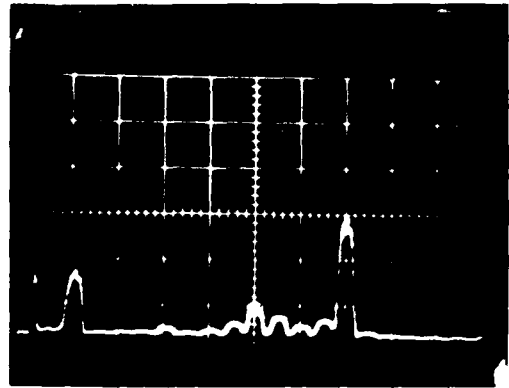
B. E-GUN

E-gun operation has taken several paths during the course of the program. We tested six cathodes. These are listed in Table 3 together with comments about the operation of each. The minimum work function obtained with vendor supplied cathodes was 2 eV while that for a normal dispenser cathode is 1.8 eV. This high work function made operation at 3 A/cm^2 impossible. The results obtained with these cathodes are now considered to have been spurious.

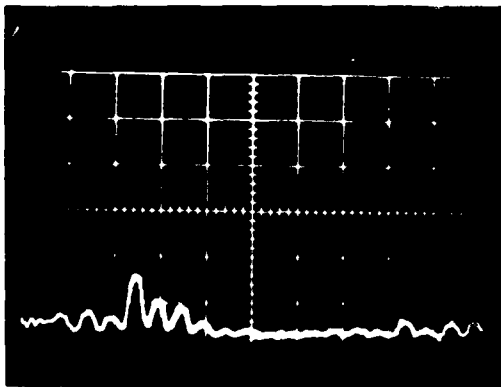
PRECEDING PAGE BLANK-NOT FILMED



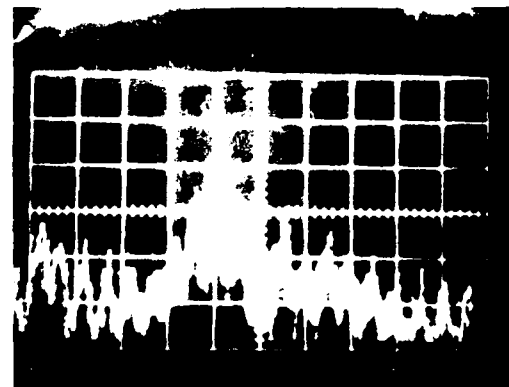
M = 10 - 30 10^{-7} RANGE



M = 30 - 50 10^{-8} RANGE



M = 50 - 70 10^{-9} RANGE



M = 70 - 90 10^{-10} RANGE

Figure 23. Mass analyzer photos.

Table 3. Tested Dispenser Cathodes

Cathode	Source	Diameter (cm)	Comments
1	Vendor	4	Heater replaced No emission in system
2	Vendor	4	Heater replaced No emission in system
3	Reimpregnated #1 at EDD	4	Low emission in system
4	Stock of standard traveling wave tube cathodes	1.3	Satisfactory emission
5	Stock of standard traveling wave tube cathodes	1.3	Satisfactory emission
6	HRL-EDD	4	Satisfactory emission

The traveling wave tube (TWT) cathodes were from a known sample batch about 20 years old. They were installed in both closed and open configurations to determine whether normal cathode operation in our vacuum chamber was possible. Space charge limited operations at over 3 A/cm^2 was observed at $>1150^\circ\text{C}$. One of these cathodes was mounted crudely in the e-gun and used to monitor the beam behavior.

Cathode number six was manufactured at Hughes. The machining of individual components was done at Hughes Research Laboratories, and the brazing and cathode impregnation was carried out at the Hughes Electron Dynamics Division. A satisfactory cathode was produced. This cathode has operated at theoretical perveance (0.15×10^{-6} perv) near 400 kV; however, the temperature required for full space charge limited emission was approximately 80°C hotter than predicted. A typical I-V characteristic curve for this cathode is shown in Figure 24. A typical current trace for near 400 kV operation is shown in

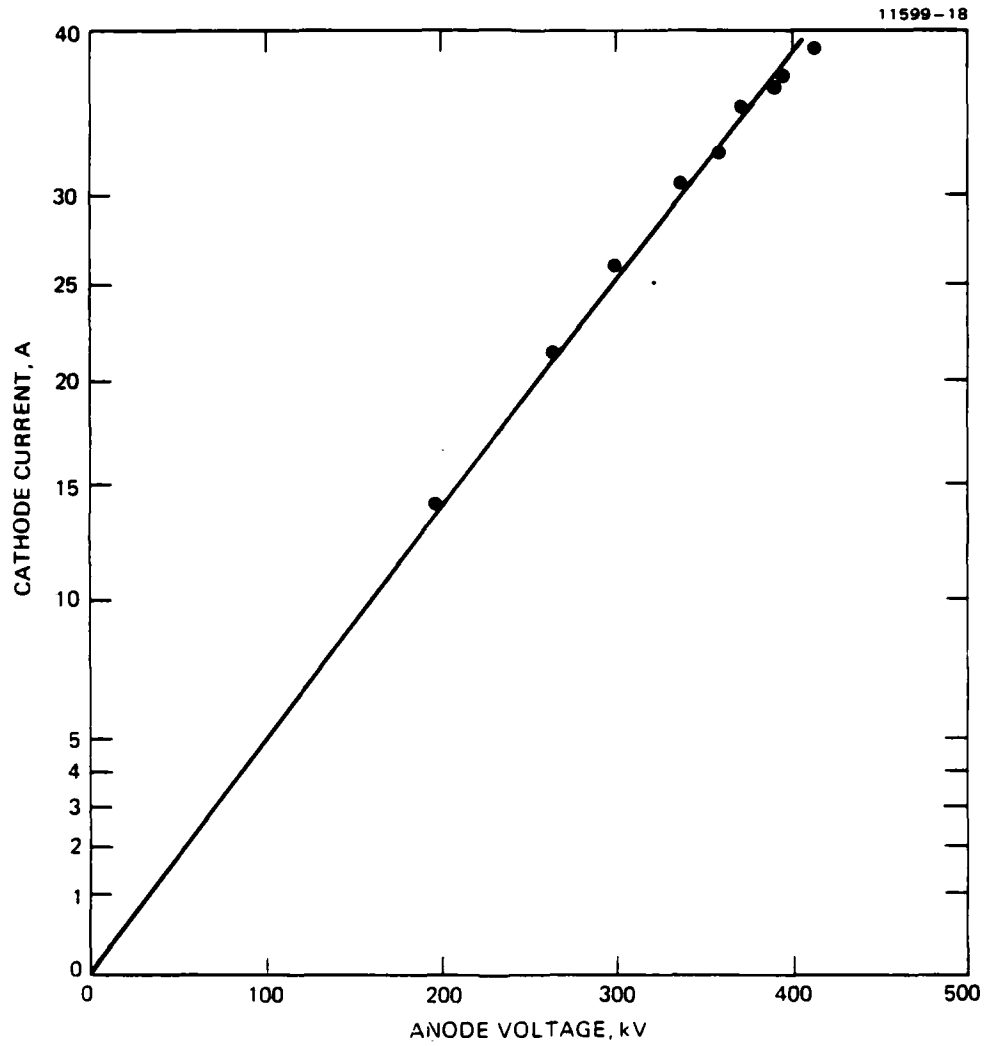


Figure 24. Current-voltage characteristic, $T_k = 1140^\circ \text{C}$.

Figure 25. The current shown here (37A) means the gun is operating at a perveance of 0.15μ perv. Operation above 300 kV must be done without a direct voltage monitor. Available voltage dividers fail above this voltage. It has been found from lower voltage testing that the capacitor charge voltage is a good measure of the final erected Marx-bank voltages.

Beam Quality Measurements

The quality of the e-beam has been crudely checked using a phosphor screen as a depressed collector. The e-beam produces an image of the cathode at periodic values of magnetic field which is photographed through the window behind the collector. Two cathodes were used in these tests; a smaller traveling wave tube cathode mounted in the cathode position and one of the early vendor supplied cathodes. The image diameter for the TWT cathode is approximately 2 cm, which corresponds to a spreading of 50 to 60%. Distortions in the image were later confirmed to have been produced by tilting of the cathode mount at higher temperatures and by the edges of the cathode which were exposed to high fields. The edges are brighter than the center and excessive curvature of the surface (which did not fit the e-gun design) produced coma intensity patterns. The photograph of the reimpregnated vendor supplied cathode indicated a lack of emission from various portions of the cathode consistent with a poisoned cathode operating in emission limited operation; but otherwise in good mechanical alignment. These data were not taken with cathode No. 6 which we assume to be in good alignment and operating within our design limits.

C. DEPRESSED COLLECTOR

Operation of the depressed collector has been examined in several regimes. These include:

1. Low voltage (19 to 50 kV) - closed collector
2. High voltage (160 to 320 kV) - closed collector
3. High voltage (160 to 400 kV) - open collector.

Each regime has distinct characteristics so they will be discussed individually.

TIME SCALE: 2 μ sec/DIV

11599-6R1

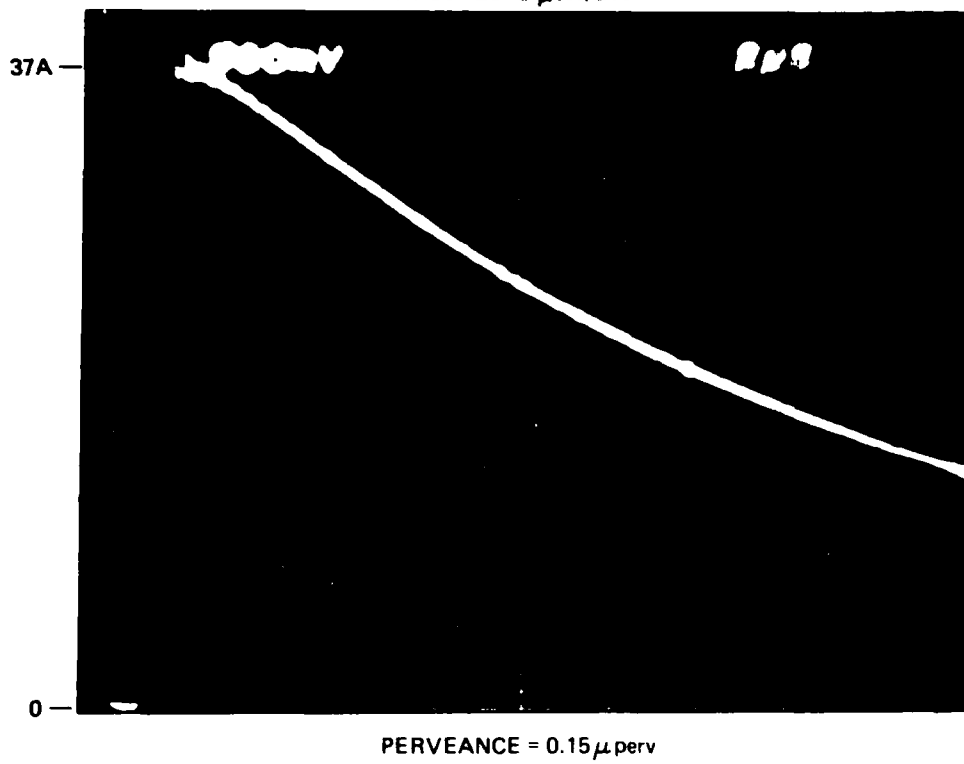


Figure 25. Typical e-gun current trace, $V_{\text{anode}} = 395$ kV.

Low Voltage

The efficiency of the single stage collector is given by $\eta = I_{dc}/I_{cathode}$ where I_{dc} is the depressed-collector current and $I_{cathode}$ is the beam current. The measurement technique is discussed in Section 4 and the expected theoretical behavior is discussed in Section 3.

Low voltage operation included data with cathodes 3 and 4. Some data was taken with the phosphor screen as the collector. This regime is characterized by strong field and voltage effects. The risetime of current in the collector is approximately 2 μ sec. The response of the collector at 19-kV beam voltage and several field values is shown in Figure 26. Trace 1 in these photographs is the depressed collector current and trace 2 is the cathode current. A solenoid current of 0.5 A corresponds to a guide field of 37 G. These photographs show that the time dependence and magnitude of collection are strongly dependent on the guide-field value. Folded into this dependence is beam voltage. A plot of depressed-collector current against delay setting or guide field for a constant beam voltage and current is shown in Figure 27. This plot shows a strong B-field dependence with distinct resonances as B is increased. Data were not taken in the neighborhood of the fourth resonance. If the solenoid current or B is plotted against mode number, as in Figure 28, a linear relationship is seen. Time constraints prevented taking data at any other mode locations.

A possible explanation for this behavior is the scalloping of the beam due to misalignment and imperfect Brillouin-flow matching. Theory says that scalloping in the beam should vary in a manner which is nearly proportional to B/\sqrt{V} where V is the beam voltage. In order for the beam to reach the collector it must first get through the exit aperture ($r = 1.5$ cm) at the end of the solenoid. Transmission will be dependent on whether the beam scallop is at a minimum or maximum. A minimum will lead to transmission to the collector. As one sweeps through values of B, maxima and minima at the aperture lead to a modal structure such as indicated by Figure 27 and Figure 28.

11344-2

I_{DC} 50 mA/DIV

$I_{CATHODE}$
100 mA/DIV

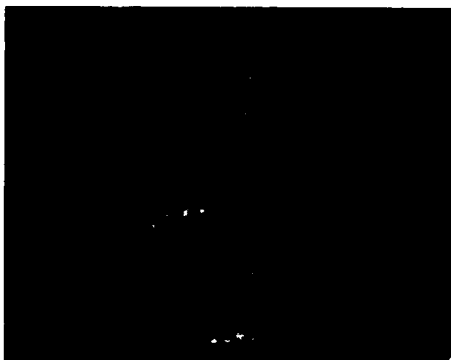


SOLENOID
CURRENT

0.45 A



0.49 A



0.50 A

TIME, 2 μ sec/DIV

Figure 26. Depressed collector response
 $V_{anode} = 19$ kV.

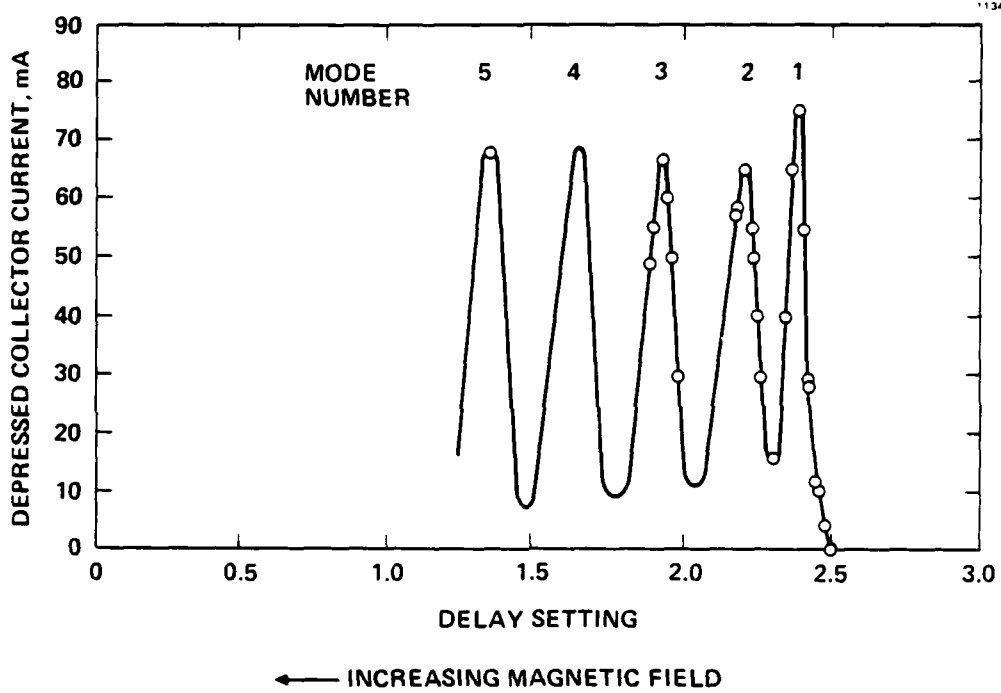


Figure 27. Depressed collector current as a function of delay setting, $V_{\text{anode}} = 19 \text{ kV}$.

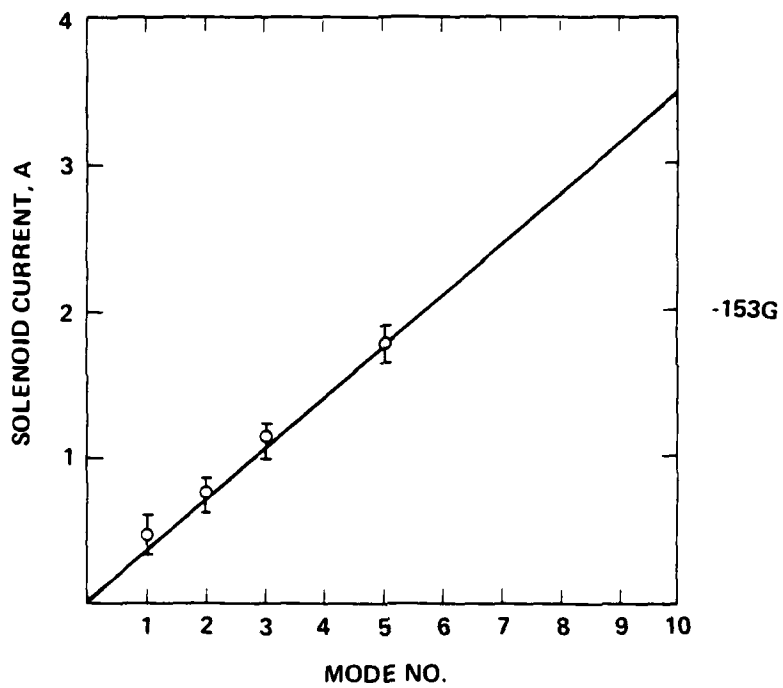


Figure 28. Solenoid current as a function of mode number, $V_{\text{anode}} = 19 \text{ kV}$.

Also at low anode voltage, the collector bias voltage was swept at constant B-field value. The results of these data are given in Figure 29 along with the secondary emission coefficient from copper.¹⁴ The expected behavior based on the code model would be for the collection to reach nearly maximum value at a collector voltage of 1% of beam voltage. It should then be reasonably constant at higher voltages. The dip seen in Figure 29 could be due to the increase in secondary emission as the voltage is swept, indicating some loss of secondary electrons. Possibly a part of the beam may be intercepted by the collector outside of the desired space-charge-depressed region producing secondaries that are lost to the anode. The dip occurs at the peak of secondary emission.

High Voltage (Closed Collector)

Of more importance to the program is high voltage operation of the gun and depressed collector. Some typical data are shown in Figure 30 and Figure 31. Figure 30 shows the change in collector response with magnetic field; a beam current trace is also shown. The collection is reasonably well behaved except at one value of B-field. Here an instability forms in the collector, due probably to collapse of the space charge. Figure 31 shows the change in the collector response as the collector voltage is changed. The noise on the beam current trace is due to ground-loop pick up of noise from the collector instability at a collector voltage of 2 kV. The step in the 2 kV trace shows the formation of the space-charge well as the beam voltage drops slightly. Space charge formation tends to begin at 1% of the beam voltage.

The important parameter of collection is the efficiency, η . This efficiency is plotted in Figure 32 as a function of anode voltage for a constant B-field (182 G) and depressed collector voltage (4.8 kV). This plot shows a trend toward increasing η with higher beam voltage. The collector efficiency has been plotted in Figure 33 as a function of B-field for 250-kV and 285-kV beams with 4.8 kV on the collector. Contrary to the extreme periodic behavior, seen with the earlier cathodes in low voltage tests, this plot shows only a mildly periodic structure.

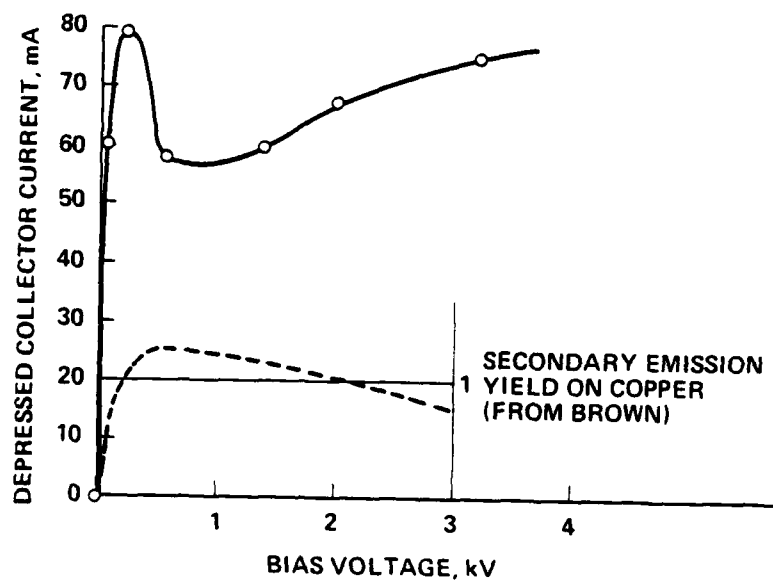


Figure 29. Depressed collector voltage dependence,
 $V_{\text{anode}} = 19 \text{ kV}$.

$V_{DC} = 4.8 \text{ kV}$
 $V_{BEAM} = 250 \text{ kV}$
 SCALE: 5A/DIV
 1 μ sec/DIV

DEPRESSED
 COLLECTOR
 CURRENT →

↓
 CATHODE
 CURRENT



363G



325G



273G



190G

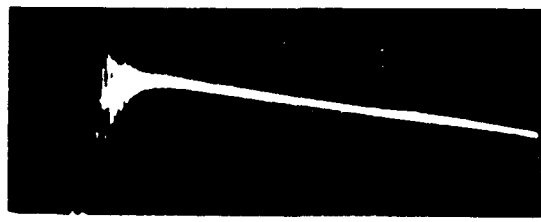
Figure 30. Depressed collector current vs. guide field strength

$B_0 = 190\text{G}$
 $V_{\text{BEAM}} = 250\text{ kV}$
SCALES: 5A/DIV
1 $\mu\text{ sec/DIV}$

DEPRESSED
COLLECTOR
CURRENT \rightarrow
CATHODE
CURRENT \downarrow



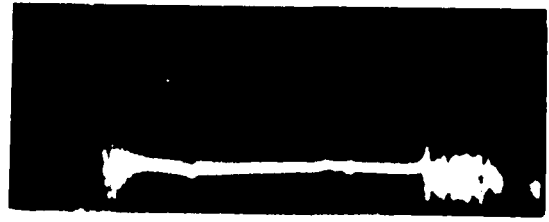
5.2 kV



3 kV



2 kV



1 kV

Figure 31. Depressed collector current vs. voltage.

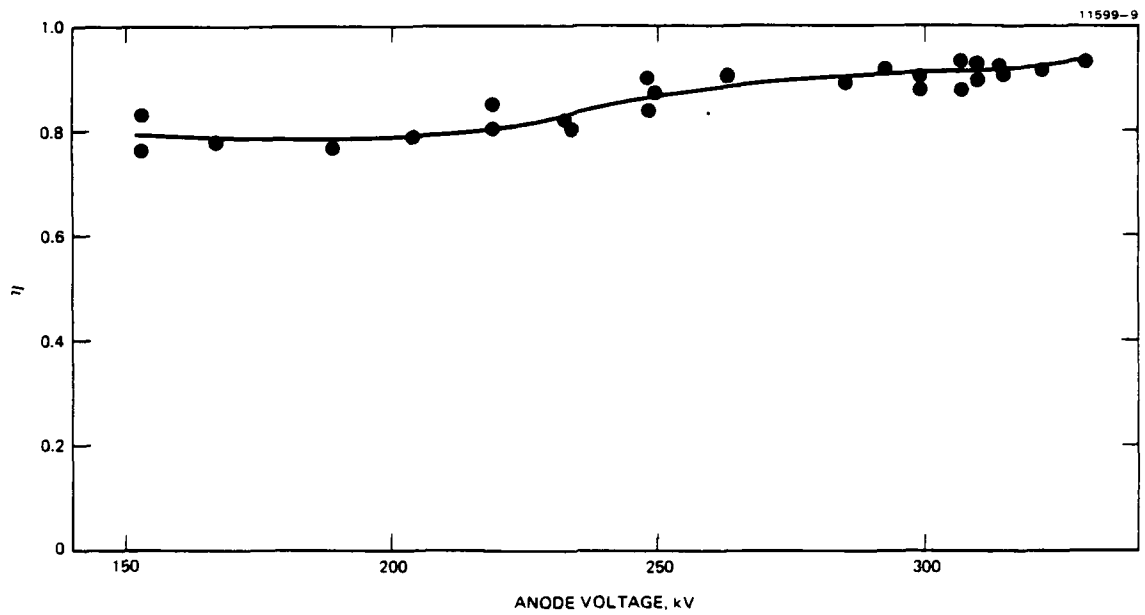


Figure 32. Depressed collector efficiency versus anode voltage.

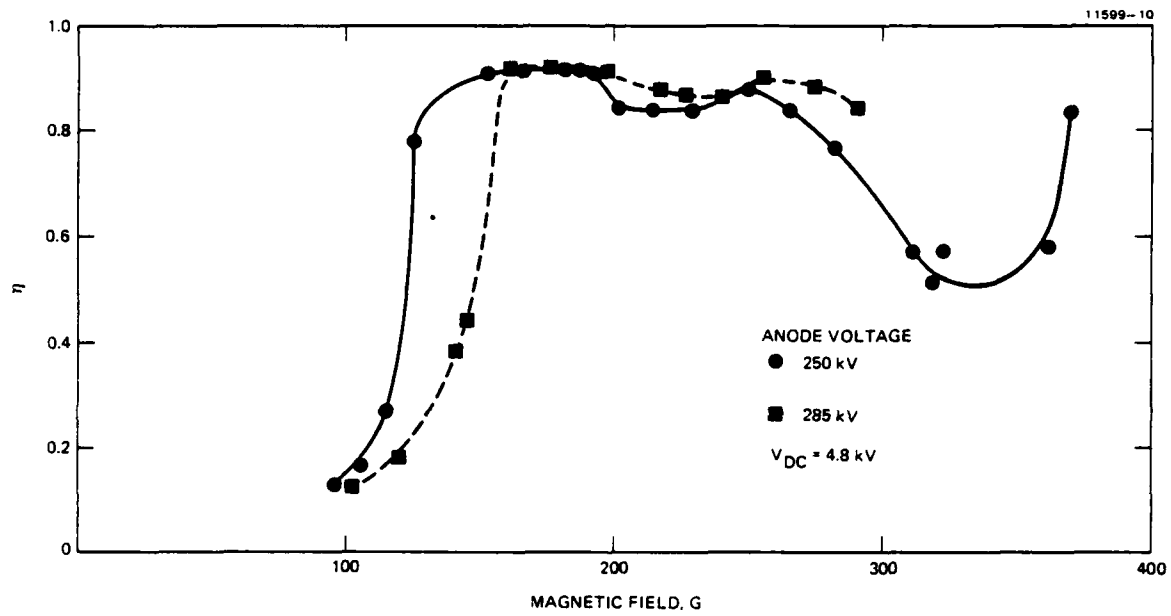


Figure 33. Collector efficiency vs. magnetic field.

A dip in the efficiency is seen near 340 G for the 250-kV case. Data above 370 G was not taken due to limitations in the solenoid driver circuit. The shape of these curves scales roughly as $\eta = f(B/B\gamma)$; where we saw five modes at low voltage, 1.4 modes would be expected at 250 kV. This is approximately what is seen; although the envelope for high η is considerably broader and higher with the correct cathode installed in the e-gun.

Finally, collection efficiency has been studied as a function of depressed-collector voltage at 250 kV and at two different magnetic field values. These data are plotted in Figure 34. At the lower B field value a sharp knee occurs at about the 1% value of beam voltage. At the higher field value, the knee is not as sharp, however, it may still be present. Some evidence of the leakage of secondary electrons is present above 1% of the beam voltage.

High Voltage (Open Collector)

Thomson scattering experiments require a hole in the depressed collector to allow probing the e-beam. A depressed collector with a hole might also be used as an output port for FEL radiation. Some testing was done with a hole in the collector for the Thomson scattering experiment. The plot of these data are shown in Figure 35 for two different beam voltages. With this collector configuration maximum collection efficiencies of only 60% were obtained. Apparently the space charge formation is inhibited by leakage through the hole. Further work must be done if collectors with holes are required; however, this was not a goal of the present project.

From the preceding discussion, it is apparent that the conditions for Brillouin flow depend on the magnetic field, the beam voltage, radius and current; whereas the conditions for high collection efficiency depend on the magnetic field, the beam voltage, and the length of the drift section. This fact suggests that future FEL system designs should take into account the possibility of simultaneously matching maximum collection efficiency with Brillouin flow.

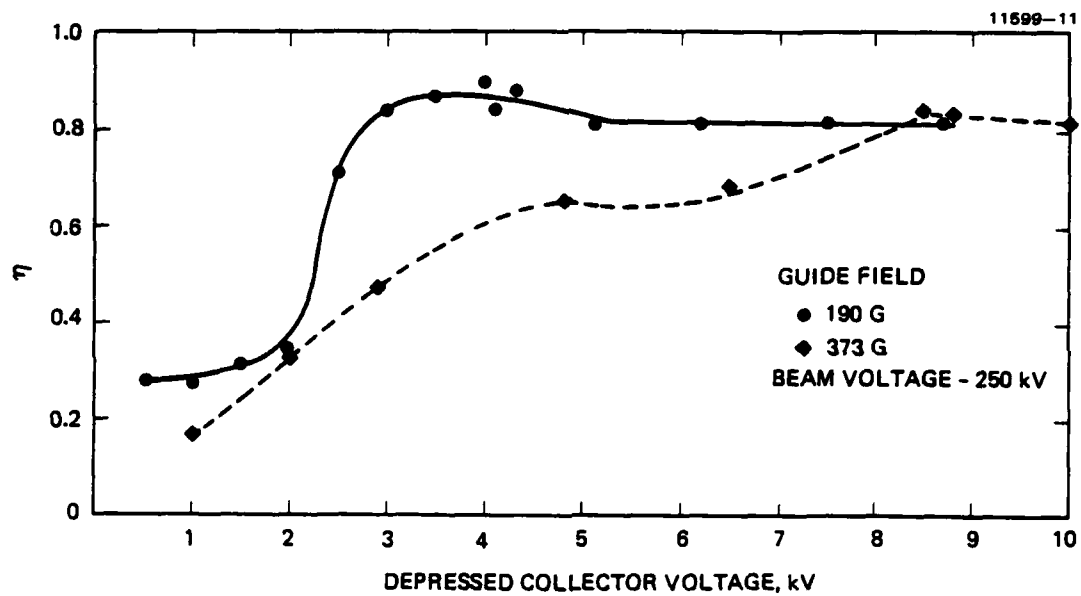


Figure 34. Depressed collector efficiency versus collector voltage.

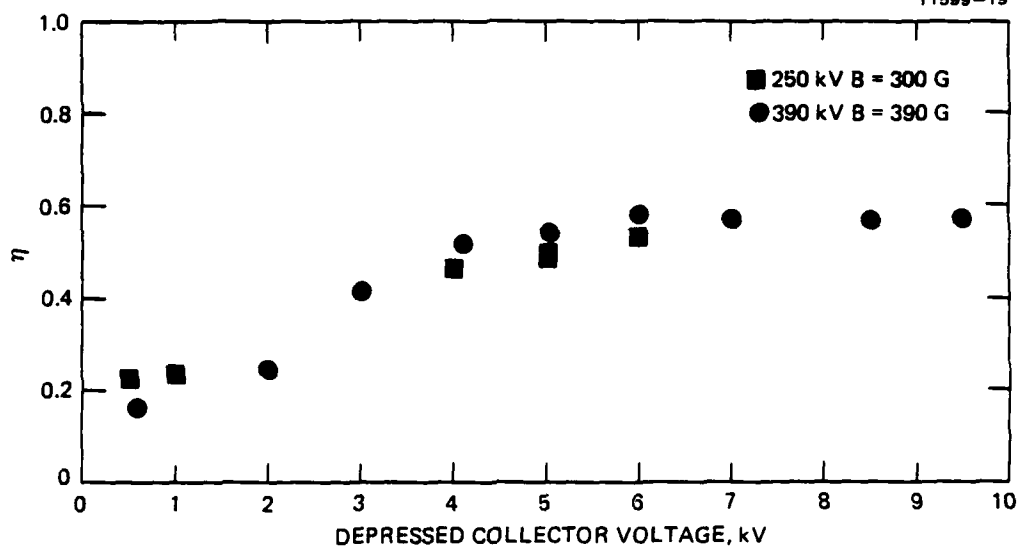


Figure 35. Depressed collector efficiency with axial hole) versus collector voltage.

The general conclusions from the above data are as follows:

1. Collection at high voltage with efficiencies greater than 90% is possible. The peak efficiency seen was 94%.
2. The guide fields necessary for good collection are much lower than those predicted for Brillouin flow. Some rearrangement of the system may be required if both are simultaneously required.
3. Near its maximum, the collection efficiency is not a strong function of magnetic field or beam voltage, therefore, off-design-point operation of future FELs will not be a problem.
4. Single electrode depressed collectors with laser output holes need to be more carefully studied before they can be used in an efficient FEL.

D. THOMSON SCATTERING

Measurement of the energy spread of the e-beam has proven to be a difficult technical challenge. Various techniques for making this measurement have been outlined in Section 4. The end-on approach chosen still presents problems in application due principally to the need to reliably operate above 400 keV. The maximum sensitivity is obtained when a photomultiplier and narrow-band interference filter are used for data collection rather than a monochromator (due to solid angle effects). However, the particular optical band chosen depends on the exact beam voltage. Using a digital voltmeter on the charging supply, an accuracy of ± 100 V ($\Delta E/E = 2.5 \times 10^{-4}$) could be expected.

A proposed solution is to dither the beam voltage by an amount at least equal to the uncertainty in voltage. However, at best, one sweep through the voltage must take place during the laser pulse which is 70 nsec wide. The minimum dither frequency is therefore 7 MHz. This requires generating a 7-MHz, 200 V signal. This concept is shown in Figure 36. The beam voltage has a dithered voltage impressed on it. During the voltage pulse, the scattered radiation is scattered into or out of the detector band. Using different band-width filters the spectral intensity can be unfolded as a function of wavelength.

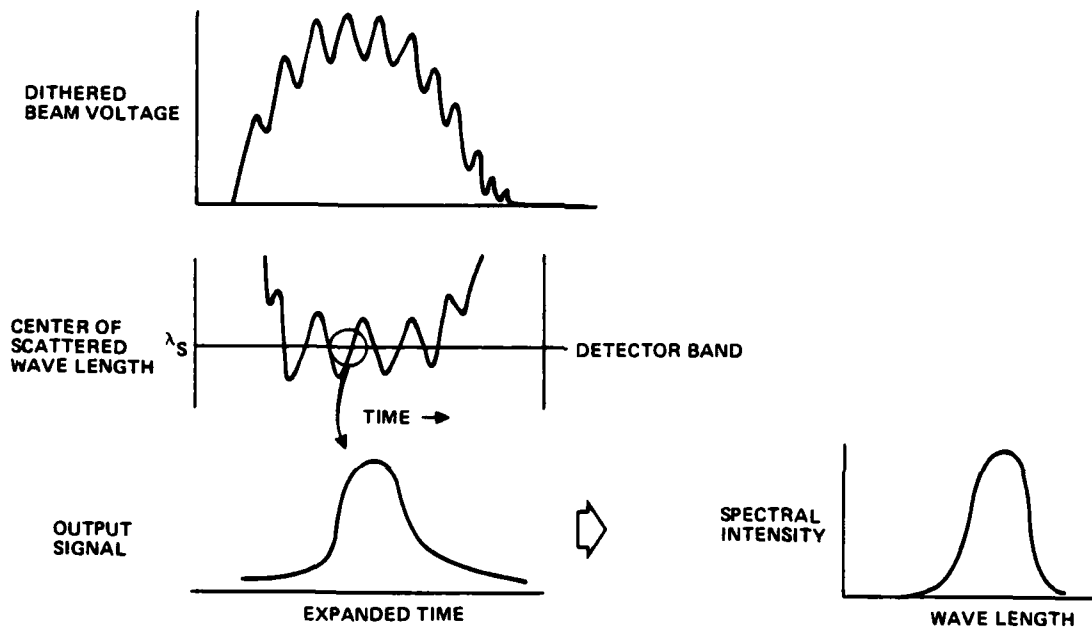


Figure 36. Thomson scattering concept.

The detector chosen for this experiment has a S-20 response. (Extended red response S-1 detectors and high quantum efficiency crystal detectors in our range of operation, while seemingly available in the literature, are no longer manufactured). If one matches the Doppler shifted laser output with photomultiplier response while folding in the efficiency of the laser with wavelength, as shown in Figure 37, an optimum operating wavelength of 9.24 μm is indicated.

The CO_2 laser is a composite of three Lumonics 101 lasers which have been mounted in an EMI shielded container. The laser has an unstable resonator with a tunable grating as a rear reflector. The grating was adjusted to the R(24) line of the $00^1 - 02^0$ transition producing a wavelength of 9.25 μm . The energy in the pulse is 3 to 4 J/pulse and pulsewidth of 70 nsec. The peak power is in the range of 20 to 50 MW. A photograph of the laser output is given in Figure 38, showing the 70 nsec pulsewidth. A beam reducer has been placed in the beam to adjust its size to approximately 1 cm. The laser beam is targeted on the central portion of the electron beam at an angle of 1° .

The optical detector uses a large diameter spherical relay mirror on the axis of the e-beam system. Ambient light from the cathode and stray room lights has not proven to be a problem.

All individual components and systems necessary for the Thomson scattering experiment have been proven to operate within the necessary ranges. Optical background light intensity (e.g., from the cathode) and background electrical noise has been reduced to a satisfactory level. High voltage conditioning of the ceramic bushings of the solenoid structure has proven to be the weak point of the system. Single shots have been accomplished at 100 kV but arcing is common and tends to damage other system components. Due to the large number of elements in the system, (which must simultaneously operate), we have elected to delay the Thomson scattering experiment until the next phase of the program, when planned improvements are to be made in the reliability of the system at 400 keV.

During the program a new conceptual approach to a two stage FEL has been developed which would reduce the $\Delta E/E$ requirements of the e-gun by over an order of magnitude. This has lowered the priority of the Thomson scattering experiment.

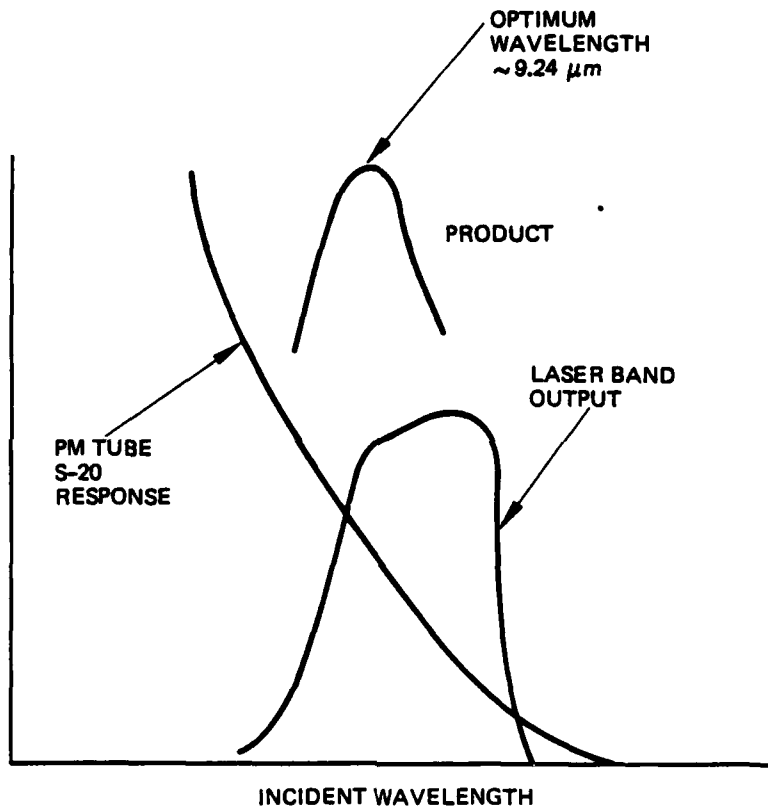


Figure 37. Detector response criteria.

11599-20



FWHM = 70 ns

Figure 38. Laser temporal response.

SECTION 7

SUMMARY

DESIGN MODELS

The Electron Trajectory Program written by W.B. Herrmannsfeldt⁵ was used as the basic design tool for the e-gun and depressed collector. A thermal electron propagation code⁸ developed at Hughes was used to examine propagation of the electron beam outside the e-gun.

A low perveance (0.15 μ pervs) e-gun was designed. The design operating point is 400 kV and 38 A. For a well designed e-gun, the major source of longitudinal energy spread in the beam is the space-charge depression. Cathode segmentation and Brillouin flow are examined as methods of reducing the effect of the space charge depression. In a practical system neither technique can completely eliminate the longitudinal energy spread. With our e-gun shape, the code predicts that these two techniques will yield the following momentum spreads ($\Delta P_z/P_z$) at the output of the gun:

- (1) segmented cathode: $\Delta P_z/P_z = 2.5 \times 10^{-4}$
- (2) Brillouin flow: $\Delta P_z/P_z = 5 \times 10^{-4}$

For systems using post acceleration of the beam to higher voltages, the momentum spreads would reduce proportionately to the relative voltage increase.

The depressed collector design was a single-stage unit using space-charge depression within the collector cup to prevent loss of secondary electrons from the collector. The space charge well was shown to form at about 1% of the beam voltage. The predicted maximum efficiency was $\eta = 0.987$.

THOMSON SCATTERING MODEL

End-on Thomson scattering has been chosen as the best candidate for measurement of the momentum spread in the electron beam. A 400-keV electron beam causes:

- (1) the scattered radiation intensity to be enhanced by relativistic effects by a maximum of 375 for on-axis scattering
- (2) the frequency of scattered radiation to be shifted by a factor of 10.6 times.

With a $9.3\text{-}\mu\text{m}$ input radiation at $5 \times 10^7 \text{ W/cm}^2$, an electron beam of density of $n_e = 10^{10} \text{ cm}^3$ will scatter 10^4 photons/pulse at $0.88 \mu\text{m}$ into an $f/20$ optical system. By looking nearly on axis, transverse velocity terms are reduced to negligible quantities.

EXPERIMENTAL RESULTS

The results of the experimental program to date are as follows:

- (1) Operation of a 400-kV, 38-A e-gun at predicted perveance has been achieved.
- (2) Depressed collection of the electron beam with efficiencies greater than 90% has been achieved. The peak measured efficiency was 94%. This means that the electrical efficiency of a FEL can be increased an order of magnitude per stage using depressed collection.
- (3) The space-charge well necessary for efficient electron collection forms at about 1% of the beam voltage as predicted by computer simulation.
- (4) The guide fields necessary for efficient collection do not match those predicted for our particular Brillouin flow arrangement. Some adjustment of the system may be required so that the Brillouin matching field and the efficient collecting field are coincident.
- (5) Collection efficiency at high beam voltage is not a strong function of either beam voltage or guide field value, therefore, off design point operation of future FELs may be practical.
- (6) Single-electrode depressed collectors with laser-output holes need more careful study before they can be used in an efficient depressed collector.
- (7) Optical and electrical background noise is at sufficiently low levels to allow the Thomson scattering experiment to be carried out.
- (8) Thomson scattering data collection will be more meaningful when modifications are made to make the system more reliable and repetitive at 400 kV.

REFERENCES

1. L.R. Elias, Phys. Rev. Lett. 42, 977 (1979).
2. N.M. Kroll and W.A. McMullin, Phys. Rev. A17, 360 (1978).
3. P. Sprangle and R. Smith, Phys. Rev. 21, 293 (1980).
4. A. Gover and P. Sprangle, J. Appl. Phys. 52, 599 (1981).
5. W.B. Herrmannfeldt, "Poisson Equation Solving Program," Stanford Linear Accelerator Center Report No. SLAC-226 (1979).
6. M. Reiser, Phys. of Fluids 20, (3), 477 (1977).
7. C. Parazzoli, submitted to Phys. Rev. A.
8. THERMR, a program developed by K. Amboss for Hughes Aircraft Company.
9. J.W. Hansen and C. Sussking, IRE Trans. on Elect. Devices 7, 282 (1960).
10. W. Neuzebauer and T. Mibrom, IEEE Trans. on Elect. Devices 19, 111 (1972).
11. J.E. Walsh, Physics of Quantum Elect. 7, 255, Addison Wesley (1979).
12. J.M. McKinley, Amer. J. Physics 218, 612 (1980).
13. H.E. Gallagher, J. of Appl. Phys. 40 (1), 44-51 (Jan. 1969).
14. S.C. Brown, Basic Data of Plasma Physics (MIT Press, Cambridge, 1967).

ACKNOWLEDGMENTS

The authors wish to acknowledge the contributions of the following persons. Computer codes and helpful suggestions were supplied by Professor W.B. Herrmannsfeldt (Stanford University) and by Dr. K. Amboss (Hughes EDD). Early consultation and support was provided by Mr. R.A. Hill. Early conceptual designs and e-gun simulations were provided by Dr. D.E. Elerath and Ms. T.L. Dobbs; early Thomson scattering analyses were performed by Dr. D.R. Fields and FEL code simulations by Dr. R.P. Korechhoff at (Hughes EODS). Mr. L.R. Falce provided consultation and coordination for the final cathode processing at Hughes EDD. At HRL initial design studies and scaling studies were performed by Dr. H.J. King with detailed designs by Mr. J.D. Rose. Dr. J. Hyman, Jr., provided general consultation support. Dr. D.K. Lynch was responsible for the design and set-up of the optical equipment for Thomson scattering. Mr. H.E. Gallagher provided extensive high voltage engineering support and was responsible for the design and construction of the Hughes cathodes. Mr. P.W. Sumner, Mr. D.R. Mize, Mr. R.L. Maheux, and Mr. R.G. Fleig provided invaluable technical, mechanical, electrical, and test support.

END